Mesoscale Variability in the Atlantic Ocean from Geosat Altimetry and WOCE High-Resolution Numerical Modeling

DETLEF STAMMER AND CLAUS W. BÖNING

Institut für Meereskunde an der Universität Kiel, Kiel, Federal Republic of Germany

(Manuscript received 22 April 1991, in final form 30 September 1991)

ABSTRACT

Characteristics of the mesoscale variability in the Atlantic Ocean are investigated by analyzing the Geosat altimeter signal between 60°S and 60°N. The rms sea-surface variability for various frequency bands is studied, including the high-frequency eddy-containing band with periods < 150 days. Wavenumber spectra and spatial eddy characteristics are analyzed over 10° by 10° boxes covering both hemispheres of the Atlantic Ocean. A comparison with solutions of a high-resolution numerical experiment, developed as the Community Modelling Effort of the World Ocean Circulation Experiment, aids interpretation of the Geosat results in the tropical and subtropical Atlantic and provides a test of the model fluctuating eddy field.

Results from Geosat altimetry show a wavenumber dependence close to k_1^{-5} (k_1 being the alongtrack wavenumber) over almost the entire Atlantic Ocean except for areas in the tropical and subtropical Atlantic where the rms variability in the eddy-containing band is less than 5 cm, that is, not significantly different from the altimeter noise level. Characteristic eddy length scales inferred from Geosat data are linearly related with the deformation radius of the first baroclinic mode over the whole Atlantic Ocean, except for the equatorial regime (10°S to 10°N).

The data–model comparison indicates that the high-resolution model with horizontal grid size of 1/3° and 2/5° in latitude and longitude is quite capable of simulating observed eddy characteristics in the tropics and subtropics. In mid- and high latitudes, however, the model fails to simulate the pronounced poleward decrease in eddy scales. This leads to systematic discrepancies between the model and Geosat observations, with model scales being up to 50% larger than deduced from altimetry.

1. Introduction

During the last 20 years considerable efforts have been made to infer characteristics of the mesoscale variability in the oceans. From current meter time series sampled during experiments like MODE (Mode Group 1978) or POLYMODE (McWilliams et al. 1983), it was possible to document frequency characteristics of the ocean mesoscale variability. For a comprehensive review the reader is referred to Wunsch (1981). Unlike frequency spectra and time scales of the ocean eddy field, the characteristics of the corresponding wavenumber spectra and spatial scales are barely known and are unexplored over vast regions of the World Ocean. Basically, this is because conventional hydrographic measurements cannot provide synoptic long-distance observations with spatial resolution capable of resolving the ocean mesoscale. Only a few rather preliminary estimates of wavenumber spectra in the Atlantic Ocean have been made from moored current-meter arrays deployed during MODE, POLYMODE, and TOURBILLON (Le Group Tourbillion 1983). Based on MODE and TOURBILLON, Mercier and Colin de Verdiere (1985) hypothesized a relationship between eddy scales and the first Rossby radius of deformation. Recently, Krauss et al. (1990) supported those results by an analysis of surface drifter motions and satellite IR images. According to them, the eddy scale decreases northward from the subtropical Atlantic and can be closely related to the Rossby radius. In the Pacific Ocean, Bernstein and White (1974, 1977) used BT and XBT measurements of temperature to estimate wavenumber spectra. From all experiments strong evidence exists that the ocean eddy field is highly inhomogeneous both in its amplitude (see, e.g., Wyrtki et al. 1976) and its frequency–wavenumber characteristics (Richman et al. 1977); this means that any result obtained locally to be nonuniversal.

Recently, the U.S. Navy's Geodetic Satellite (Geosat) has provided an altimetric dataset with unsurpassed space–time sampling characteristics that offers large potential for studying oceanic mesoscale variability. Because satellite altimetry provides quasi-synoptic, long-distance measurements of the sea surface height (SSH), with an alongtrack resolution of the order of 10 km, its space–time resolution is superior to all conventional oceanographic measurements. The

Corresponding author address: Dr. Detlef Stammer, Institut für Meereskunde an der Universität Kiel, Dusternbrooker Weg 20, Kiel 1 D 2300, Federal Republic of Germany.

potential of satellite altimetry for studying the ocean mesoscale had been demonstrated with data of the earlier *GOES-3* and Seasat missions (e.g., Cheney et al. 1983; Douglas et al. 1983; Fu 1983a; Gordon and Baker 1980; Menard 1983). See Fu (1983b) for an extensive review on application of satellite altimetry to study the ocean mesoscale. Using Geosat data, Fu and Zlotnicki (1989, hereafter FZ) repeated previous studies on ocean wavenumber specta. Similar to Fu (1983a), they basically obtained two mean wavenumber spectra that represent ocean areas of "high" and "low" eddy kinetic energy, respectively.

According to FZ, areas of high eddy activity can be characterized by one-dimensional wavenumber (k_1) spectra following a k_1^{-5} power law roughly for wavelengths between 100 and 300 km. This result appears consistent with the theory of geostrophic turbulence (Charney 1971; Rhines 1979), which predicts a k^{-3} spectral dependence of eddy kinetic energy assuming geostrophy this corresponds to a k^{-5} slope for SSH. For the low-energy areas, however, a well-defined energy-containing band could not be documented and the wavenumber spectra were represented by a spectral power law of k_1^{-2} for wavelengths smaller than about 1000 km. This result is puzzling, since it implies a white eddy kinetic energy spectrum over vast areas of the World Ocean. In the North Atlantic Ocean the low eddy energy area as specified in Fu (1983a) extends from 20° to 60°N, east of 40°W, and includes the North Atlantic Current (NAC). To explain the marked difference of spectral characteristics between "high" and "low" eddy energy areas, Fu (1983a) hypothesized a stronger effect of linear Rossby wave dynamics in the low energy areas. Recently, LeTraon et al. (1990) investigated the North Atlantic mesoscale variability poleward of 20°N by calculating wavenumber spectra and autocorrelation functions in spatially limited areas extending 10° in latitude and longitude, respectively. They also found a distinct geographic dependence of wavenumber spectra, predominantly of latitude, which they attributed to differences in eddy forcing and to different dynamical regimes.

We feel that at least two effects have been omitted in the previous discussions. The first, relevant to the results of FZ, is the impact of track length, which when extending over long distances in latitude, serves to average over different eddy scales; the second is the noise level of Geosat data, which in the very low energy areas of the subtropics may mask the oceanic signal. It will be shown later that both represent important factors in interpreting results from altimeter data, and it needs to be studied whether spectral power laws as reported in the literature indeed resemble the oceanic signal or to which degree they reflect uncertainties inherent in the altimetric analysis procedure.

In this analysis we use 58 repeats of Geosat altimeter data to investigate characteristics of the ocean mesoscale eddy field in the Atlantic Ocean between 60°S and 60°N. Specific questions that will be addressed are:

- Is there a systematic geographical dependence of the predominant eddy scale similar to that of the first baroclinic Rossby radius of deformation?
- To what extent is the mesoscale variability governed by a universal wavenumber spectrum?

To reinforce our conclusions about physical processes that lead to the oceanic spectra, the results from Geosat will be compared to the solutions of a high-resolution numerical model of the North Atlantic Ocean.

The model of the equatorial and North Atlantic had been developed as the Community Modelling Effort of the World Ocean Circulation Experiment (WOCE). It is based on the primitive equation model of the wind-driven and thermohaline circulation of Bryan (1969) and Cox (1984). Building upon the initial 25-year experiment of Bryan and Holland (1989) at NCAR, a sequence of model runs focusing on the model sensitivity to frictional parameterization and wind forcing was conducted both at NCAR and IfM Kiel (Böning et al. 1991). Various model–data comparisons have demonstrated the capability of the model to produce the salient features of the current system in the tropical and subtropical Atlantic (Spall 1990; Didden and Schott 1992; Schott and Böning 1991) but indicated specific deficiencies in high latitudes; for example, in simulating the Gulf Stream position (Bryan and Holland 1989), or the level of eddy kinetic energy in the northeastern Atlantic (Treguier 1992). In this study we investigate the spatial characteristics of the model surface pressure fluctuations using similar methods as for the altimeter analysis. It will be shown that model results can aid the statistical interpretation of altimeter measurements in the subtropics where the rms variability barely exceeds the data noise level, and that the eddy characteristics derived from altimeter observations provide a powerful tool to test results of a large-scale numerical model.

In section 2 we briefly describe the Geosat data analysis procedure and the configuration of the numerical model. The pattern of mesoscale variability and wavenumber spectra inferred from Geosat data over the Atlantic Ocean between 60°S and 60°N are presented in section 3, where reasons leading to disagreements with respect to previous publications will also be discussed. A comparison of eddy statistics as inferred from Geosat and model data is given in section 4, and implications concerning a close relation between the oceanic eddy scales and the first internal Rossby radius of deformation are discussed in section 5. A summary and conclusions follow in section 6.

2. Database and method

The analysis of the mesoscale variability in the Atlantic Ocean is based on more than 2½ years of alti-

meter data from the U.S. Navy's Geodetic Satellite's (Geosat) Exact Repeat Mission (ERM). Results from the altimeter observations are compared to those inferred from WOCE/CME high-resolution numerical modeling.

a. Geosat altimeter data

A total of 58 repeats of Geosat ERM altimeter data are used to study characteristics of oceanic mesoscale variability in the entire Atlantic Ocean between 60°S and 60°N latitude, 100°W and 40°E longitude. Corresponding to the 17.05-day repeat period, the data cover the period from 8 November 1986 to 20 July 1989. The spatial resolution from ascending and descending tracks is about 7 km alongtrack and 165 km zonally close to the equator. The cross-track separation reduces substantially toward high latitudes. See Cheney et al. (1987) for a description of the Exact Repeat Mission and the Geophysical Data Records (GDR).

We used the collinear method (Cheney et al. 1983) to analyze the sea surface height (SSH) anomalies relative to a 2-year reference mean (the first 43 repeats). Prior to the collinear analysis the data were interpolated onto a fixed alongtrack grid with a resolution of 6.8 km corresponding to the 1-Hz sampling rate. Various environmental corrections supplied with the GDRs were applied to the data including the ionospheric and the dry and wet tropospheric path delay [the latter two taken from the Fleet Numerical Oceanographic Center (FNOC)], and sea level fluctuations due to solid earth and ocean tides. The sea state bias was corrected by 2% of the significant wave height; we likewise corrected fluctuations in atmospheric load assuming isostatic ocean response. Remaining "blunder" points were edited. Because tidal corrections are somewhat uncertain for continental shelf regions any data for ocean depths less than 1000 m were excluded (see Fig. 1a). During the collinear analysis procedure care has to be taken to avoid the mean estimate to be biased by data gaps due to the large orbit error (4 m rms). The reader is referred to Willebrand et al. (1990) and Didden and Schott (1992) for a detailed description of the method and a discussion of the applied corrections.

To analyze the Geosat data over the entire Atlantic Ocean, the collinear method was applied separately in subareas, each extending over 40°–50° in latitude. Neighboring areas were chosen to overlap by 10° in latitude, in order to minimize border effects. In each subdomain the radial orbit error was removed using a quadratic polynomial over arc lengths typically 5000 km long. Whenever the track length was less than 1000 km, a bias and trend was used instead. No filtering was applied to the data prior to the derivation of statistical quantities like rms sea surface variability or wavenumber spectra.

Inherent in the Geosat data analysis are some critical error sources, which should be kept in mind when interpreting results. Perhaps the most serious degradation of the dataset comes from the lack of synoptic measurements on board Geosat of the path delay due to tropospheric water vapor. Therefore, information from external sources provided with the GDRs have to be used. Mesoscale variability of tropospheric water vapor content, however, fails to be properly resolved by the FNOC (Fleet Numerical Oceanography Center) analysis. In FZ, the residual water vapor error from Seasat measurements was analyzed; they conclude that the latter has much less variance, on average, than found from Geosat data on the mesoscale. Yet, strong individual water vapor anomalies may occasionally affect sea surface height anomalies. Recently new sets of more accurate water vapor corrections have become available (Emery et al. 1990; Wentz 1990). While they show major discrepancies relative to the FNOC corrections especially in the tropics, it is only the difference relative to a mean profile that matters for the purpose of this study. Therefore, the influence of the water vapor (wv) correction on Geosat results can be expected to be only of minor importance; for example, the variation of eddy scales estimated from the first zero crossing of mean autocorrelation functions in the tropical Atlantic (0°–20°N, 20°–30°W) varies by no more than 10% when using 1) no water vapor corrections, 2) FNOC, and 3) the new estimation of wv provided by Wentz (1990). The influence of tropospheric wv correction on Geosat altimetry in the Atlantic Ocean is currently under investigation (Didden and Stammer 1992).

It is noteworthy that the analysis procedure itself contains error sources associated with subtraction of a least-square polynomial during the radial orbit error correction. This procedure can create a bias, especially when large-amplitude anomalies associated with boundary current meanders are present simultaneously with a reduced arc length due to gaps in the data.

b. Numerical model of the North Atlantic

The numerical model of the wind-driven and thermohaline circulation is based on the primitive equation model described by Bryan (1969) and Cox (1984). It covers the geographical domain between 15°S and 65°N, 100°W and 14°E with spatial grid resolution of 1/3° in latitude and 2/5° in longitude. In the vertical, it has 30 levels. The initial experiment performed by Bryan and Holland (1989) at NCAR was a 25-year simulation starting from initial conditions as given by the climatology of Levitus (1982). A sequence of model runs was performed at IfM Kiel, focusing on the model sensitivity to changes in model parameters like wind forcing and friction coefficients (Böning et al. 1991).

In the Bryan–Cox model surface gravity waves are filtered out by applying a rigid-lid approximation at the upper boundary, and the model is formulated in a way such that the surface pressure gradient is not required during the course of the integration. It can, however, be recovered diagnostically from the prog-

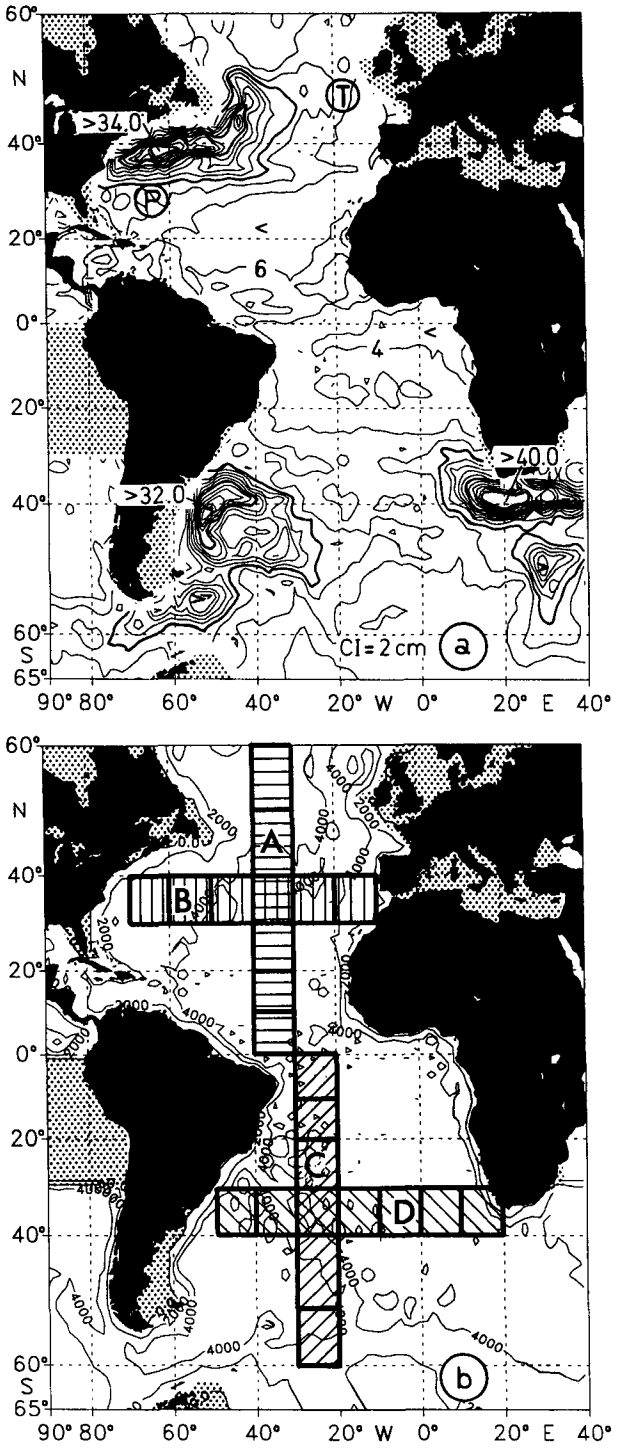

FIG. 1. (a) Rms sea surface variability from 58 repeats of Geosat ERM altimeter anomalies (8 November 1986 to 20 July 1989) estimated in 2° by 2° areas. Labels P and T mark POLYMODE and TOUBILLON experimental sites from which surface streamfunction statistics are used for comparison (see Fig. 8). Contours exceeding 30 cm are suppressed; contour increment is 2 cm. Stippling indicates areas with no data processed during this study. (b) Number of valid Geosat data in 2° by 2° areas. Hatched regions mark sections labeled A to D, from which results are shown in Figs. 6 and 9. Contour increment 2000.

nostic model variables. Subsequently, the surface pressure can be computed by integrating its horizontal gradients over the model domain. The integration constant is determined by imposing zero mean surface displacement, that is, conservation of mass. We used three years of surface pressure taken every third day from a model run that was driven by the monthly mean wind stress climatology of Isemer and Hasse (1987). For details on friction coefficients see Böning et al. (1991) (experiment Kiel #2). For the comparison with Geosat observations, we converted the three years of surface pressure fields into their equivalent surface elevations, assuming hydrostatic balance in the form

$$\zeta(x, y, t) = \frac{1}{g\rho_0} p(x, y, t) \qquad (1)$$

where ζ is the surface elevation, p the surface pressure, g the earth gravity constant, and ρ_0 is a mean density. In this study we are interested only in the surface variability rather than the mean circulation. Therefore, the total surface elevation is decomposed into a mean and a fluctuating part:

$$\zeta(x, y, t) = \bar{\zeta}(x, y) + \zeta'(x, y, t). \qquad (2)$$

Only the deviation ζ' from the 3-year mean $\bar{\zeta}$ has been analyzed during this study. Note that ζ' is the Geosat data equivalent due to the lack of any permanent signal in the Geosat anomaly fields.

3. Results from Geosat altimetry

From the 2½ years of Geosat SSH anomalies, we calculated area-averaged mean wavenumber spectra and autocovariance functions from which integral length scales of the ocean eddy field have been estimated. Likewise, frequency spectra and eddy time scales are studied. Size and locations of geographical subdomains for estimating statistical quantities of the mesoscale ocean eddy field were chosen to be consistent with the spatial inhomogeneity of the sea surface variability.

a. Sea surface variability

The rms sea surface variability calculated from 58 repeats of Geosat SSH anomalies (8 November 1986 to 20 July 1989) in geographical boxes each spanning 2° in latitude and longitude is given in Fig. 1a; the number of valid observations in each of those boxes is displayed in Fig. 1b. The pattern and amplitude of variability are consistent with previous publications; such as Koblinsky (1988) or Zlotnicki et al. (1989). Minor differences can be attributed to different evaluation periods and to details of the analysis procedures. Figure 1a demonstrates that the spatial distribution of

surface variability is highly inhomogeneous. It compares qualitatively with the distribution of eddy kinetic energy drawn, for example, from historical ship drift data (Wyrtki et al. 1976) and from surface drifter motion (Richardson 1983). There is high variability along major current systems, like the Gulf Stream in the North Atlantic and the Brazil–Falkland confluence and the Agulhas Current in the Southern Hemisphere. Maximum variability is found to be associated with the Agulhas current with rms values reaching 40 cm. In the vicinity of the Gulf Stream the rms variability reaches values of 35 cm at 40°N, 62°W and in the Brazil–Falkland confluence maximum numbers exceed 32 cm at about 40°S, 50°W. Enhanced variability is found also along the extensions of the boundary current in the North Atlantic, that is, the North Atlantic Current (NAC) (8 cm–20 cm) and the Azores front (>6 cm).

Minimum variability occurs along latitude bands through the center of the subtropical gyre of both the Northern and the Southern hemispheres. In the North Atlantic the rms variability is less than 5 cm between 10°N and 30°N. In the Southern Hemisphere the low variability area is shifted equatorward by about 10° in latitude; values of less than 6 cm extend across the basin between 20°S and the equator. Sailor and LeSchack (1987) estimated the Geosat instrumental noise level to be about 3 cm; this number corresponds to the minimum variability of about 3 cm found in the Guinea Basin. Similar to eddy potential energy (Dantzler 1977; Emery 1982), the sea surface variability increases both pole- and equatorward from the subtropics. The maximum variability in the tropical Atlantic occurs somewhat south of 10°N, at about 40°W; it is associated with the variability of the equatorial current system (see the following for further discussion).

In the Southern Hemisphere, the enhanced variability in zonal bands between 45°S and 48°S, and close to 30°S, is associated with the current system in the South Atlantic Ocean; that is, the Antarctic Circumpolar Current (ACC), which traverses the Atlantic basin roughly between 50°S and 45°S downstream of the Brazil–Falkland confluence, and the Agulhas retroflection area south of Africa. A detailed review on the South Atlantic current system may be found in Gordon (1988). Based on Geosat SSH anomalies, Gordon and Haxby (1990) documented the separation of eddies from the retroflecting Agulhas Current that subsequently moves in a westward direction close to 30°S. The enhanced variability south of the Agulhas Current at about 50°S, 30°E is consistent with estimates of eddy kinetic energy from drifting buoy observations. They show a pronounced increase in eddy activity in the region where the ACC passes the Atlantic–Indian Ridge (Daniault and Menard 1985; Piola et al. 1987). Likewise enhanced variability is present in numerical modeling results (Semtner and Chervin 1990). The variability in the region south of the ACC is fairly low with numbers being less than 6 cm.

It may be noteworthy to hint at some structures associated with the Gulf Stream variability in the North Atlantic. The variability is fairly low over the Blake Plateau and increases downstream of Cape Hatteras. Maximum values occur east (downstream) of the New England Seamounts (NES), which closely agrees with observational evidence from drifter trajectories (Richardson 1983). Auer (1987) analyzed the position of the Gulf Stream landward surface edge from five years of infrared AVHRR imagery. He reported low cross-stream excursions of the northward-flowing jet upstream of Cape Hatteras; this corresponds to the low variability of SSH anomaly in the Geosat data. The cross-stream excursion increases significantly after the stream has separated from the continental shelf. It obtains maximum values at about 38°N, 65°W in close agreement with the location of the variance maximum from altimetry. A secondary maximum in SSH variability (>22 cm) is present along the core of the NAC north of Flemish Cape. There is evidence that the sharp water mass boundary along that current, separating cold Labrador water from warm subtropical waters, is a major energy source for mesoscale eddy activity (Krauss et al. 1990). The variability associated with the NAC decreases notably in zonal direction downstream from that location.

In general, oceanographic variability can be caused by a wide range of processes with a wide range of time scales, including seasonal variations, meandering currents, or mesoscale eddies. The variability displayed in Fig. 1a is a composite of contributions with periods shorter than the observational period of about 2½ years. It comprises not only the eddy-containing band in the period range 50 to 150 days (Richman et al. 1977), but also variability on longer time scales, such as annual and interannual. In addition, any residual environmental error that has not been corrected properly during the collinear analysis procedure contributes to the total variability. As mentioned above, this holds in particular for any error of the tropospheric water vapor correction that can have a significant influence, especially in the tropical Atlantic.

To separate the mesoscale ocean variability from longer-period signals, we calculated the rms surface variability from filtered input data using a Hanning high-pass filter with a cutoff half-power period of about 150 days. Figure 2a gives the resulting high-frequency (eddy) variability from Geosat observations. Mean values of the total and high-frequency variability, zonally averaged between 40° and 20°W, are given in Fig. 4. The geographic distribution of the eddy signal is quite similar to that of the total variability. Maximum eddy variability is associated with boundary current systems; it is about 20% less than the total variability in the Gulf Stream area and the Brazil–Falkland confluence. In the Agulhas current, up to 90% can be explained by the eddy activity. However, a large fraction of the variability in the tropical Atlantic and along the Azores front is on longer than eddy time scales.

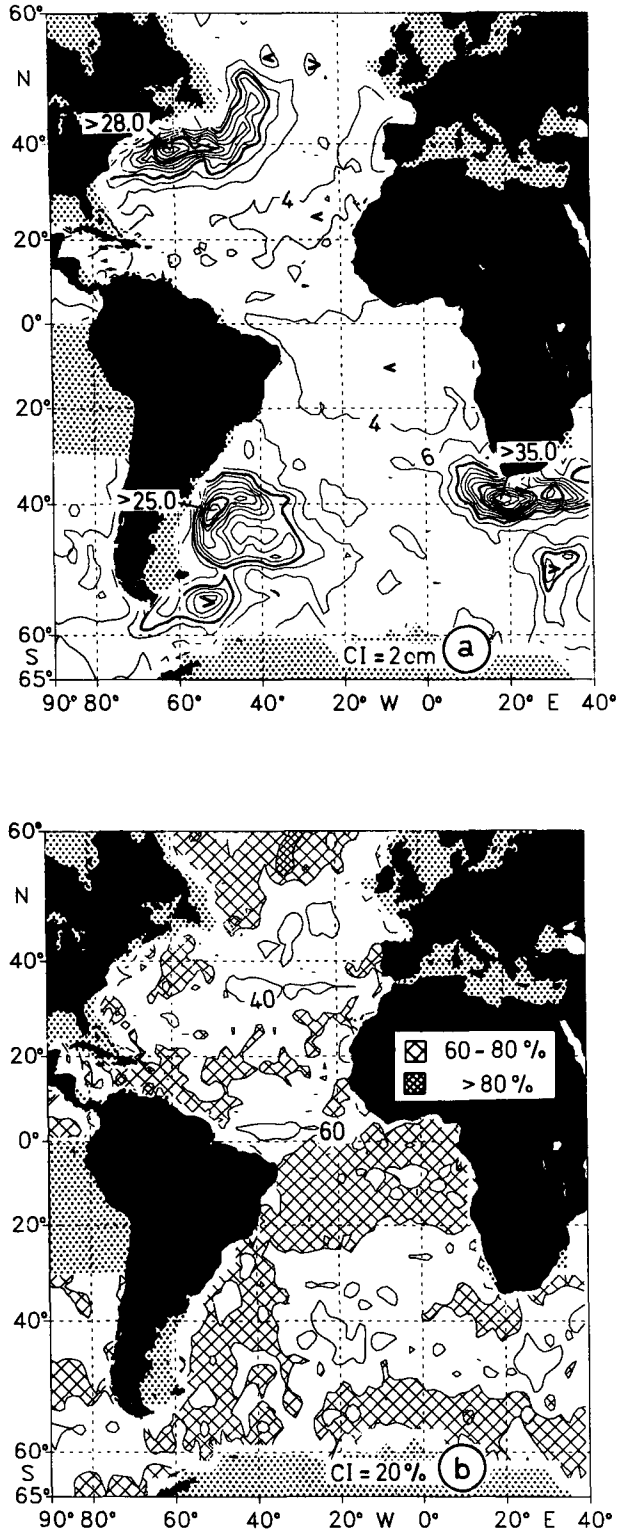

FIG. 2. (a) Same as Fig. 1a, but Geosat high-frequency variability in the eddy-containing band with periods less than 150 days. Values are calculated from high-passed Geosat anomalies by applying a Hanning spectral data window. (b) Percentage variability explained by the Geosat high-frequency variability. The contour interval is 20% for contours larger than 40%. Percentage exceeding 60% and 80% are hatched light and dark, respectively.

Between 20°S and 30°N, the rms variability is less than 4 cm; it is only marginally enhanced (4–5 cm) in the tropical band 0°–10°N. Thus, the eddy variability in that area is not significantly different from the data noise level (indicated by stippling).

The percentage of the total variability that can be explained by the high-frequency part is given in Fig. 2b. Areas with more than 60% variability due to eddies have been hatched. They are basically associated with areas of high eddy activity along boundary currents. However, high percentage south of 40°S is not associated with the variability along the ACC as seen from Fig. 1a but is shifted poleward by about 10°. The same holds upstream of Drake Passage, where the ACC also tends to be dominated by longer-period motions, while eddy motion dominates poleward and equatorward of the ACC. In the North Atlantic, high percentage of eddy motion covers the area along the subarctic front and north of it. In the tropics, enhanced percentage can be found along the coast of northern Brazil in agreement with results from historical ship drift data (Richardson and McKee 1984) from which enhanced eddy activity has been reported along the coast of Brazil.

There is a large area in the South Atlantic equatorward of 20°S with a strikingly high percentage of high-frequency variability across the entire basin. Since this area coincides with that of low total variability, this may partly reflect an increased degradation of the altimeter data due to measurement noise.

A similar but weaker pattern of high percentage occurs in the North Atlantic central subtropical gyre along a belt between the Canary Basin and the Caribbean. From hydrographic measurements this area is known to be characterized by enhanced values of eddy potential energy (Dantzler 1977; Emery 1983); favorable conditions for baroclinic instability processes are indicated by the distribution of potential vorticity (Keffer 1983; Gill et al. 1974; McDowell et al. 1982). From numerical modeling the westward-flowing portion of the subtropical gyre is likewise known to be a source of baroclinic instability (Cox 1985).

The contribution of the annual variability was estimated by calculating the annual harmonic from two years of monthly mean SSH anomaly maps produced by averaging the alongtrack data in 2° by 2° boxes (Fig. 3). This averaging filters out small-scale structures with time scales less than the annual harmonic. Basically, contributions owing to the annual harmonic exceeding 40% of the input variability (from gridded data) occur only in the tropical and subtropical Atlantic equatorward of 10°S and of 25°N. Maximum percentage of the annual harmonic occurs in zonal bands roughly along 5°N and 15°N, respectively; values exceed 80% at about 5°N, 30°W. A strong contribution of the annual harmonic was inferred also in the Geosat data analysis of Didden and Schott (1992), who attributed it to seasonal changes of the equatorial current system.

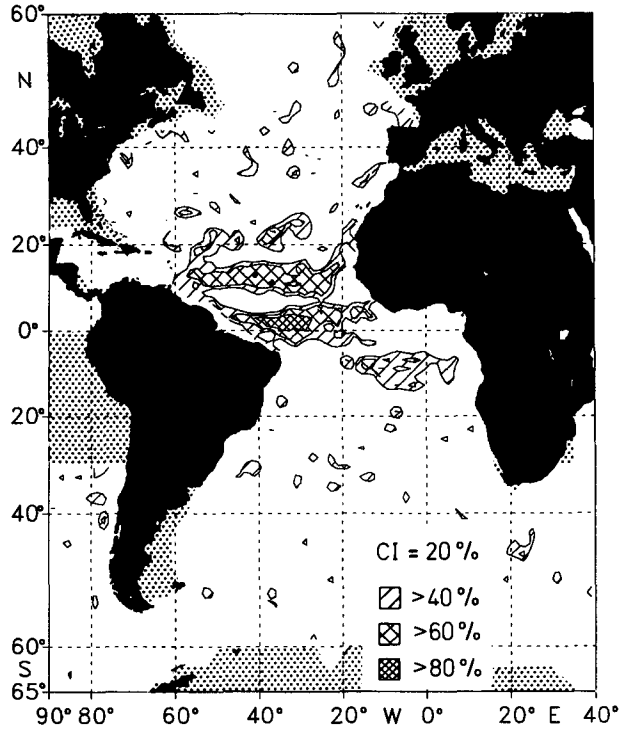

FIG. 3. Percentage variability explained by the annual cycle. Values are estimated from 24 monthly mean Geosat anomalies gridded on 2° by 2°. Contour interval is 20%. Percentage exceeding 40%, 60%, and 80% are hatched light, medium, and dark, respectively.

b. Alongtrack wavenumber spectra

To meet statistical requirements and to avoid averaging over areas dominated by different eddy dynamics, we calculated alongtrack wavenumber spectra $E_1(k_1)$ in various 10° by 10° subdomains, which cover the Atlantic basin as indicated in Fig. 10. To examine the influence of the length of track segments, results were tested against those from larger areas spanning 20° and 30° in latitude and longitude. Given isotropic conditions, the scalar wavenumber spectrum $E_0(k)$ and the kinetic energy spectrum $F_0(k)$ can, in principle, be estimated from the alongtrack wavenumber spectrum $E_1(k_1)$. Here k denotes the scalar wavenumber and k_1 denotes the alongtrack wavenumber. Examples for $E_0(k)$ and $F_0(k)$ are given in Fu (1983a) and LeTraon et al. (1990). In this study, however, we restrict the analysis to the alongtrack wavenumber spectrum. Instead, we provide an estimate of the wavenumber spectrum in two roughly orthogonal directions by considering ascending and descending tracks separately.

In Fig. 5 area-averaged wavenumber spectra from ascending (solid curve) and descending (dashed curve) tracks are given for three different parts of the North Atlantic Ocean, representing the Gulf Stream extension at 30°–40°N, 60°–70°W (Fig. 5a), the central subtropical gyre at 20°–30°N, 40°–50°W (Fig. 5b), and the equatorial current system at 0°–10°N, 30°–40°W (Fig. 5c), respectively. The spectra from ascending and descending tracks in the three areas agree within the confidence limits. It likewise holds for the entire Atlantic Ocean that no significant differences in the spectral estimates from ascending and descending tracks can be found. There are marked differences in spectral characteristics between the three areas, which may be considered to represent different dynamical regimes. The spectra representing the high-variability area of the Gulf Stream extension (Fig. 5a) are characterized by a distinct cutoff wavenumber, corresponding to a wavelength of about 300 km. In agreement with results from FZ, the drop in energy between wavelengths of about 300 km and 100 km can be represented by a power law not significantly different from k_1^{-5}.

According to the theory of geostrophic turbulence (Charney 1971; Rhines 1979) the kinetic energy spectrum should be characterized by a k^{-3} power law for wavelengths smaller than the generation scale of the eddies. Given isotropic conditions the same power law should apply to the alongtrack spectrum of cross-track velocity. Due to the geostrophic relation of the surface current field, the theory hence implies a k_1^{-5} power law for the spectrum of the sea surface height field. The most unstable wavelength of the baroclinic instability process is given by $L_R = 2\pi R_i$, where R_i is the first internal Rossby radius of deformation. Included in Fig. 5 are values of L_R as given by Emery et al. (1984), averaged over the corresponding areas; in case of Fig. 5a, L_R is about 200 km.

The spectra representing the tropical Atlantic (Fig. 5c) are somewhat less steep than in Fig. 5a, and there is no plateau at the small wavenumber end of the spectrum. To examine to what degree the spectral estimates from 10° × 10° areas in the tropics are representative of the small wavenumber end, we calculated the combined spectrum from both ascending and descending tracks within a 20° by 20° area extending from 0° to 20°N and 30° to 50°W. The spectrum, included in Fig. 5c (bold curve), shows no significant difference at the high wavenumber end but tends to flatten at wavelengths exceeding 900 km.

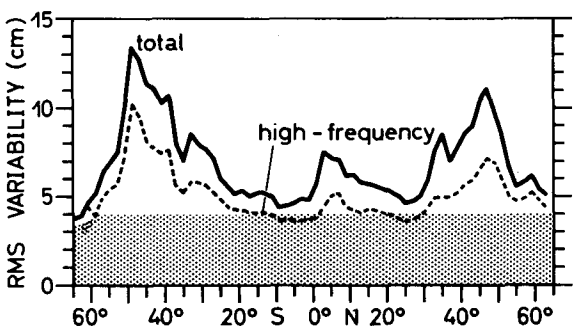

FIG. 4. Geosat zonally averaged sea surface variability between 20° and 40°W: total (solid line) and high frequency (dashed line). Values less than 4 cm are stippled to roughly indicate the data noise level.

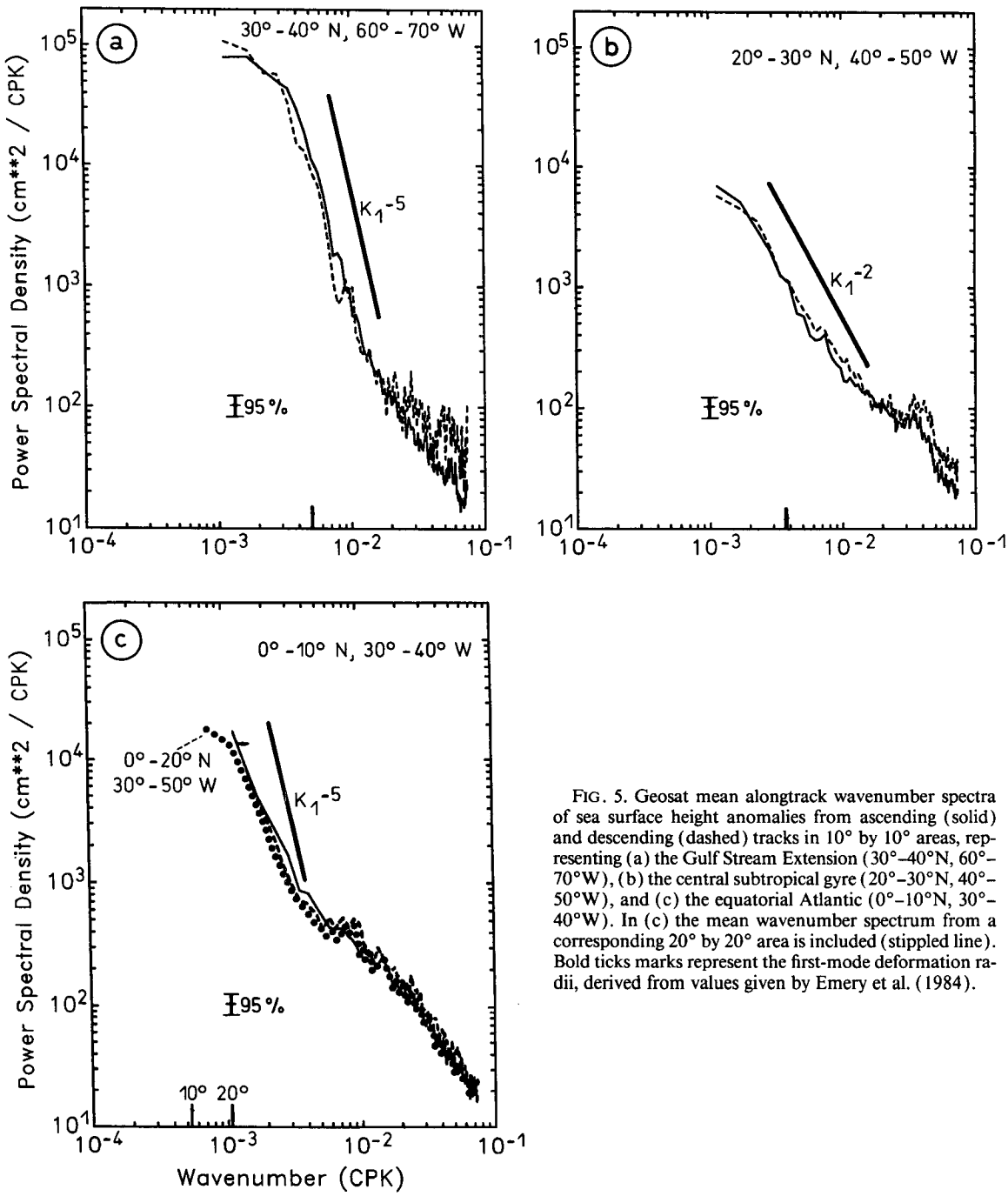

FIG. 5. Geosat mean alongtrack wavenumber spectra of sea surface height anomalies from ascending (solid) and descending (dashed) tracks in 10° by 10° areas, representing (a) the Gulf Stream Extension (30°–40°N, 60°–70°W), (b) the central subtropical gyre (20°–30°N, 40°–50°W), and (c) the equatorial Atlantic (0°–10°N, 30°–40°W). In (c) the mean wavenumber spectrum from a corresponding 20° by 20° area is included (stippled line). Bold ticks marks represent the first-mode deformation radii, derived from values given by Emery et al. (1984).

In contrast to the other two areas, the spectra representing the central subtropical gyre (Fig. 5b) show no distinct cutoff wavenumber and can be represented by a k_1^{-2} slope over the entire wavenumber range, except for wavelengths smaller than 80 km, where data noise becomes predominant. The areal extent and nature of this regime, which appears to be characterized by a white energy spectrum, will be elucidated in the following.

An important feature of the eddy variability is the decrease of the predominant wavelength toward higher latitudes. This behavior is exemplified in Fig. 6, which shows mean wavenumber spectra from ascending tracks averaged over 10° by 10° areas along four sections (labeled A to D; see also Fig. 1b), traversing both hemispheres of the Atlantic Ocean in zonal and meridional direction, respectively. An increase of the spectral cutoff wavenumber with latitude is obvious in

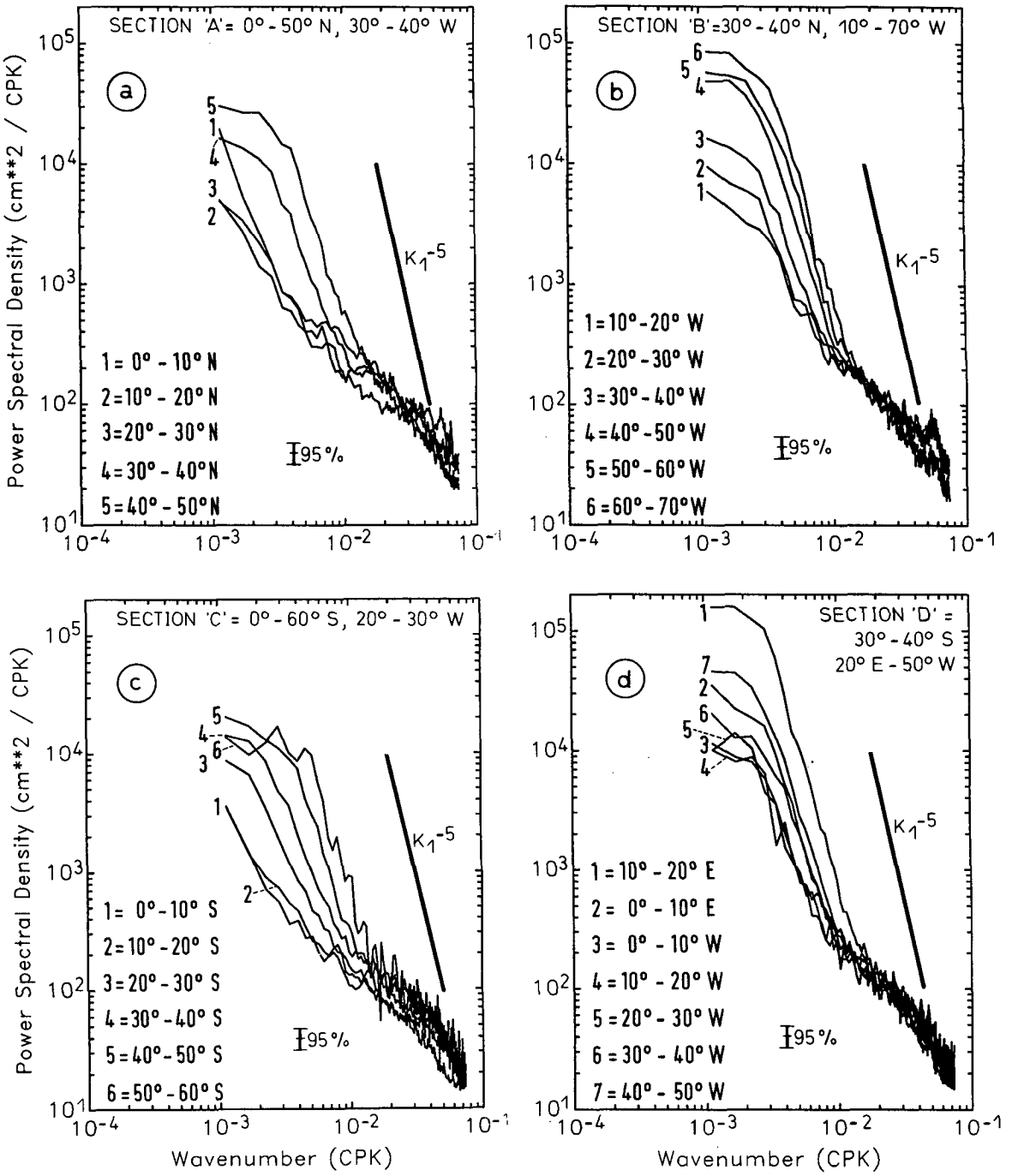

FIG. 6. Geosat mean alongtrack wavenumber spectra of sea surface height anomalies (ascending tracks only) in 10° areas following section A to D; see Fig. 1b for the course of the sections.

the Northern Hemisphere section along 35°W (Fig. 6a); it is even more clear in the Southern Hemisphere along 25°W (Fig. 6c). It should be noted that the spectral slope appears close to −4 to −5 over large areas of the basin. Exceptions, with weaker slopes, are confined to areas with low data quality. Basically, those are the subtropical oceans in both hemispheres, 10° to 30°N and 0° to 20°S, where the rms eddy sea surface variability was found to be less than 5 cm (Fig. 4). Corresponding to the asymmetry of the variability pattern with respect to the equator, the Southern Hemisphere regions characterized by k_1^{-2} spectral relations are shifted equatorward by 10° with respect to the corresponding regions in the North Atlantic. Another region

where it is difficult to interpret the spectra are the high latitudes (50°–60°) in both hemispheres (e.g., see Fig. 6c). Due to the small eddy scales there, the spectral gap between the cutoff and the noise-contaminated high wavenumber regime becomes very small. Therefore, those areas are excluded from further considerations of spectral shapes.

In contrast to the meridional variation in eddy scale, no significant change can be seen in spectral characteristics in zonal direction (Figs. 6b and 6d). In both Northern and Southern hemispheres the spectra along 35° latitude exhibit a plateau at wavelengths exceeding about 300 km; spectral slopes beyond the cutoff wavenumber may all be characterized by a k_1^{-5} relation. Differences in the wavenumber spectra document an increase in eddy energy toward boundary current regimes rather than changing characteristics of eddy scales. Unlike the midlatitude North Atlantic (Fig. 6b), where high variability is associated primarily with the Gulf Stream at the western boundary, in the South Atlantic (Fig. 6d) both sides are characterized by high eddy activity, associated with the Brazil–Falkland confluence and the Agulhas Current.

The geographical dependence of wavenumber spectra found in our analysis stands in marked contrast to the results of Fu (1983a) and FZ, who reported weak spectral slopes over vast regions of the Atlantic Ocean. We find spectral slopes of about k_1^{-4} to k_1^{-5} in areas that are characterized in FZ by spectral relations of k_1^{-2}. This marked difference can be understood as a consequence of the monotonic decrease of the eddy scale in poleward direction. Estimating alongtrack spectra over long track segments, spanning 30° latitude or more, amounts to an averaging over spectra with different cutoff wavenumbers. This ultimately leads to a decrease in spectral slopes as demonstrated in Fig. 7. Relative to individual spectra estimated from 10° track segments, slopes reduce significantly when averaging over 20° or 30°, respectively.

We do find spectra with a similar weak relation of k_1^{-2} as reported by FZ for areas of low eddy kinetic energy only in the subtropics where the rms eddy variability is less than 5 cm. As mentioned above, the signal-to-noise ratio is very low in that part of the ocean. Hence, it remains unclear whether those spectral characteristics really represent an oceanic signal or have to be regarded as an effect of measurement noise.

c. *Spatial autocorrelation functions and characteristic scales*

From the estimates of alongtrack wavenumber spectra we calculated autocovariance functions $c(s)$ that are related to the wavenumber spectra by their Fourier transforms

$$c(s) = \int_{-\infty}^{\infty} E_1(k_1) e^{2\pi k_1 s} dk_1. \qquad (3)$$

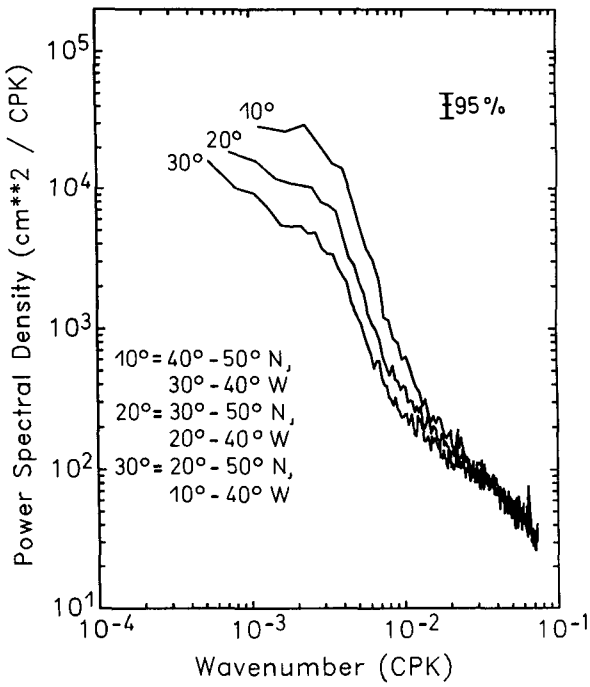

FIG. 7. Geosat mean alongtrack wavenumber spectra from three different areas extending 10°, 20°, and 30° in latitude and longitude, respectively.

In the tropics and subtropics, measurement noise on scales smaller than 60 km was suppressed by low-pass filtering before calculating the autocovariance functions. From the autocovariance function $c(s)$ integral length scales were calculated that may be considered to represent characteristic length scales of the oceanic eddy field. Instead of estimating the integral scale

$$L_\infty = \frac{1}{c(0)} \int_0^\infty c(s) ds \qquad (4)$$

from finite length data, it has become common to use modified definitions (i.e., Richman et al. 1977). In this study we calculated the two scales given by

$$L_1 = \frac{1}{c(0)} \int_0^{L_0} c(s) ds \qquad (5)$$

$$L_2 = \frac{1}{c^2(0)} \int_0^{s_{\max}} c^2(s) ds, \qquad (6)$$

where L_0 is the lag of the first zero crossing; the maximum lag $s_{\max}$ is taken to be half of the track length.

Figure 8 displays the autocorrelation functions from ascending (solid line) and descending (dashed line) tracks for two selected areas, representing (a) the western (20°–30°N, 60°–70°W) and (b) northeastern (40°–50°N, 10°–20°W) Atlantic Ocean. As seen from spectra, there are no significant differences between ascending and descending tracks. Included in Fig. 8 are two curves from analytical functions (bold lines) that

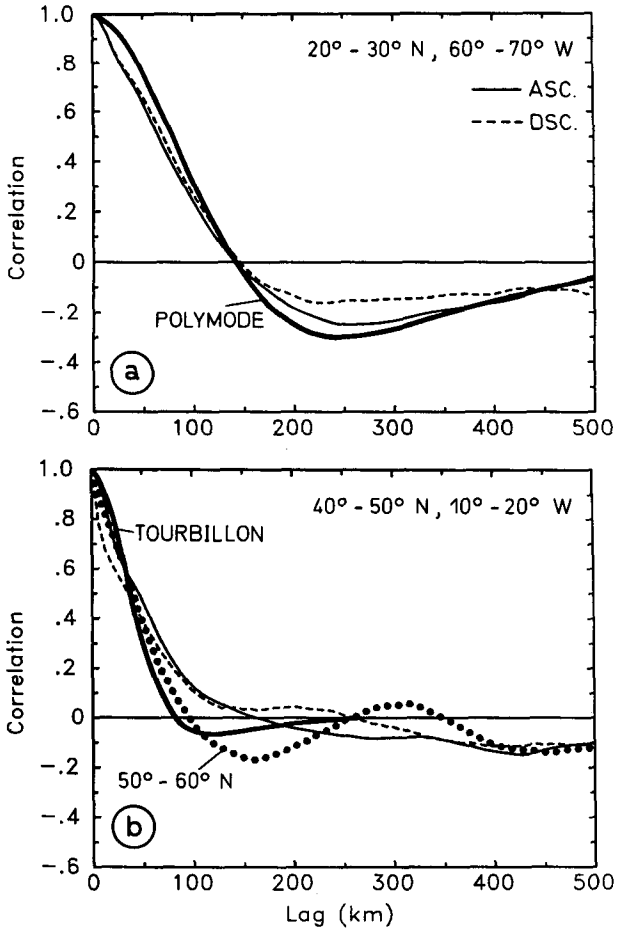

FIG. 8. (a) Geosat mean autocorrelation function from ascending (solid line) and descending (dashed line) tracks in the 10° by 10° area 20°–30°N, 60°–70°W. Included is the analytic autocorrelation function (bold line) representing typical POLYMODE sea surface streamfunction statistics (DeMey and Robinson 1987). (b) Same as Fig. 8a, but for the area 40°–50°N, 10°–20°W. The bold line represents typical TOURBILLON surface streamfunction statistics (Arhan and Colin de Verdiere 1985). Included is the alongtrack autocorrelation function (stippled line) of the area 50°–60°N, 10°–20°W, which fits the analytic function more closely.

represent the local statistics of the surface dynamic topography in those areas as estimated from POLYMODE (DeMey and Robinson 1987) and TOURBILLON moored current-meter data (Arhan and Colin de Verdiere 1985). For the POLYMODE area the agreement between Geosat results and in situ measurements is surprisingly close; differences in the shape of the curves lead to somewhat different values of integral scales; however, the first zero crossing L_0 is about the same from Geosat (139 km) and POLYMODE (140 km). In the northeastern Atlantic the eddy scales from the Geosat data are larger (L_0 = 163 km) than those from the in situ data (75 km). However, the TOURBILLON experimental site (47°N, 15°W) was close to the poleward edge of our 10° area. Therefore, we included the autocorrelation function from the next area poleward (dotted line), which indeed fits to the analytic TOURBILLON function more closely (L_0 = 96 km). LeTraon et al. (1990) reported eddy scales somewhat smaller than our results. From their Fig. 7 we deduced L_0 to be about 125 km. We do not have an explanation for the somewhat uncertain lag of the first zero crossing in this region. Those from the areas to the west (see Fig. 10) are more consistent with the numbers from LeTraon et al. (1990). The general agreement between autocorrelation functions derived from Geosat data and analytic functions estimated from (local) in situ measurements serves to increase confidence into the spatial eddy characteristics derived from altimeter measurements.

Mean autocorrelation functions from 10° by 10° areas along sections A to D are given in Fig. 9. A pronounced decrease in correlation scale toward high latitudes is found both in the Northern (Fig. 9a) and the Southern hemispheres (Fig. 9c). The lag of the first zero crossing L_0 decreases by more than 50% from 250 km near the equator to 90 km at 60°N. A similar tendency, from 260 to 90 km, can be seen in the South Atlantic.

Despite the spectral filtering in the tropics and subtropics, the corresponding autocorrelation functions are still distorted by the measurement noise (instrumental error plus small-scale environmental error residuals), leading to anomalously rapid drops of the correlation at small lags. In the Northern Hemisphere the degradation is maximum in the subtropics between 10° and 30°N; in the South Atlantic between 20°S and the equator. In agreement with Fig. 6, basically no change in eddy scales can be inferred in zonal direction along 35° latitude in both Northern (Fig. 9b) and Southern hemispheres (Fig. 9d). The curves from all subareas agree within the error bars, and there is only a slight indication of a decrease in eddy scales close to boundary currents.

A compilation of linear (L_1) (top row), quadratic (L_2) (middle row) integral scales, and zero crossing (L_0) (bottom row) from ascending and descending tracks in all 10° by 10° areas, is given in Fig. 10. In addition to the latitudinal dependency there is some tendency toward larger scales in the basin interior. This holds especially for L_0 which, for example, varies along 35°S by about 10% from the basin center toward the boundary currents. Zonal averages of L_1, L_2, and L_0 are displayed in Fig. 11. Each box comprising no pronounced zero crossing (marked by brackets in Fig. 10) has been omitted from averaging. Overall, there is a close correspondence between both hemispheres. The decrease in eddy scales tends to be symmetric about the equator, except for the range 0° to 10°N, where the zero crossing occurs at a slightly smaller scale than in the Southern Ocean. In general, estimates of eddy scales based on the linear (L_1) and quadratic (L_2) form are similar, although L_1 shows a systematic tendency toward larger values and L_2 to more spatial variation. It is important to note that, owing to the noise in the

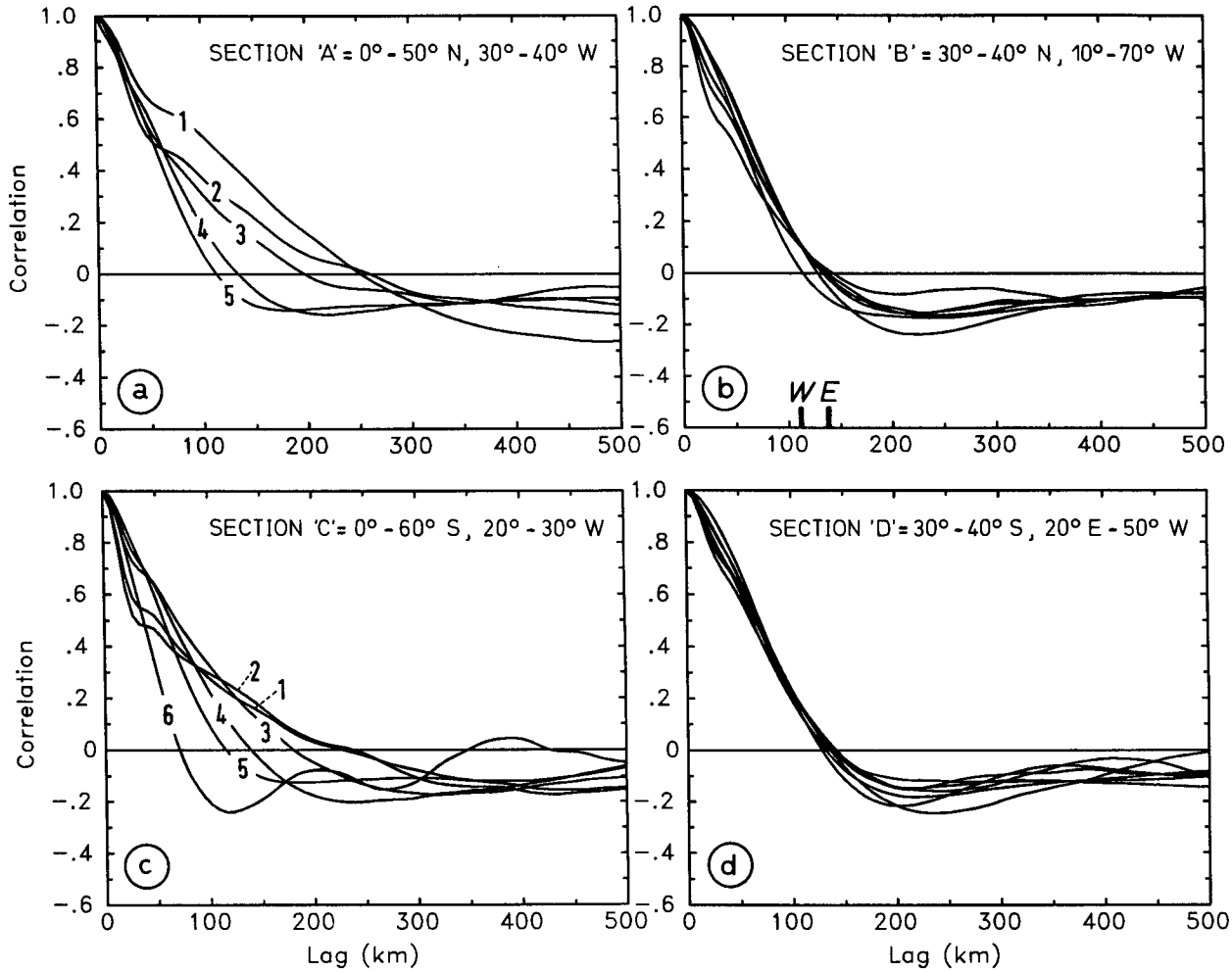

FIG. 9. Same as Fig. 6, but for the alongtrack autocorrelation function. For labels in Figs. 9a and 9c, see Figs. 6a and 6c. In Fig. 9b, E and W mark the zero crossing of the curves representing the most eastern and western area along 35°N.

Geosat measurements, eddy scales tend to be systematically underestimated between 20°S and 30°N when using integral scales. Accordingly, the zero crossing increases much faster than L_1 and L_2 equatorward of 30° latitude.

The close correspondence between estimates of linear and quadratic eddy scales is illustrated in Fig. 12, which gives a scatter diagram of L_2 against L_1 for the whole Atlantic. South of 30°S and north of 30°N (marked by asterisks) both scales show a close linear relation $L_2 = -31.5 + 1.4L_1$; the correlation is 0.93. At 30°S and 30°N a clear break appears in this behavior, and a different linear relation $L_2 = 16.9$ km $+ 0.7\ L_1$ is found in the tropics, with smaller correlation (0.79).

4. Model–data comparison of eddy characteristics

In this section the characteristics of the eddy field as inferred from Geosat observations will be compared with results of the high-resolution numerical model of the North and equatorial Atlantic. The model results will be used to reinforce our conclusions about physical processes that lead to spectral characteristics from Geosat observations. More extensively, however, we will demonstrate that the Geosat results do indeed provide a critical test of the model eddy field and its space–time characteristics.

a. Model sea surface variability

In Fig. 13a an instantaneous field of the total model sea surface elevation is shown. The northward-flowing Gulf Stream with its meandering extension and a broad recirculation are visible. Figure 13b shows the corresponding fluctuating eddy field after subtraction of the 3-year mean (Fig. 13c). Enhanced eddy activity is visible along the western boundary north of the Florida Current, extending along the Gulf Stream and the NAC into the Irminger Sea. Enhanced eddy activity is also visible along the predominantly southwestward and westward-flowing recirculation in the eastern and sub-

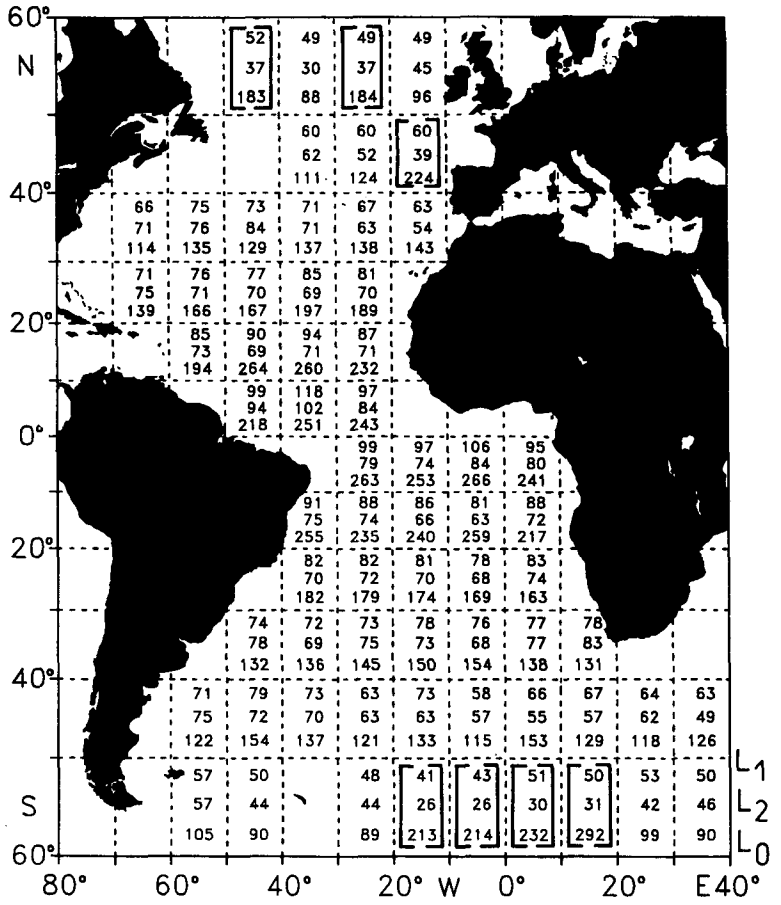

FIG. 10. Geosat spatial characteristic eddy scales, estimated from ascending and descending tracks in 10° by 10° areas. Each box contains values of the linear (L_1; top number), and the quadratic (L_2; central number) integral scale, and the lag of the first zero crossing L_0 of the alongtrack autocorrelation function (bottom number). Brackets mark areas with no well-defined zero crossing.

tropical model domain. Rather low eddy activity can be found in the central subtropical gyre and in the European basin. From Fig. 13 it can readily be concluded that the model surface elevations are rather small as compared to altimeter observations. Their amplitudes roughly agree with Geosat observations in the Gulf Stream near Cape Hatteras (see, e.g., Willebrand et al. 1990), where maximum amplitudes of about one meter can be found. However, the model amplitudes decrease rapidly in the downstream direction, and east of 60°W Gulf Stream meanders and eddies become rather weak.

Similar to the Geosat data analysis, the rms surface variability was calculated in 2° by 2° areas using three years of model surface elevation anomalies (Fig. 14a). For comparison the corresponding Geosat results are redrawn for the same area in Fig. 14b. The model rms variability is high along the Gulf Stream; maximum amplitudes of about 27 cm are found at about 70°W, 35°N where the separating stream forms a large quasi-steady loop current before turning into the basin. Secondary maxima are found north of Flemish Cap, where the NAC turns eastward, and in the Irminger Sea southeast of Cape Farewell. Enhanced variability is also found in the tropical Atlantic with maximum values off the coast of Brazil at 10°N owing to the retroflecting North Brazil Current (NBC), which turns toward the North Equatorial Counter Current (NECC) during summer and sheds eddies along the continental coast. The model evaluation of Schott and Böning (1991) shows a good correspondence of the surface currents with observational evidence in the equatorial region. Didden and Schott (1991) found a rather close agreement between model results and Geosat data in this region.

While there is a first-order correspondence between the geographical distribution of the rms surface displacement from the model and Geosat data, systematic differences are obvious in higher latitudes. The Gulf Stream variability decreases too rapidly in the downstream direction; east of 60°W there are basically no values exceeding 8 cm, in marked contrast to the observed maximum rms variability of more than 35 cm downstream of the NES. A further marked model dis-

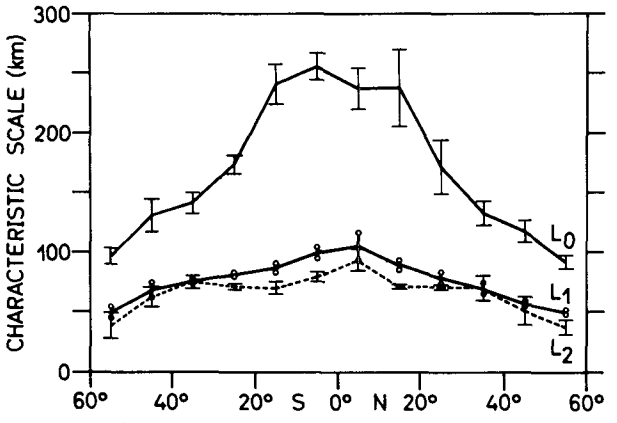

FIG. 11. Geosat zonal averages of linear (L_1) and quadratic (L_2) integral scales and lag of the first zero crossing (L_0) given in Fig. 10. The error bars indicate the conrresponding standard deviations from zonal averaging.

crepancy is associated with the NAC in the northern North Atlantic, which is shifted westward by about 20°. High variability found in the model along 40°W north of 50°N corresponds to enhanced variability in the European basin east of 20°W in the Geosat data. The model variability is much too low (up to a factor of 4) in the central and, in particular, in the eastern North Atlantic.

In order to separate the eddy signal from variability at longer periods, a Hanning high-pass filter with cutoff period of about 150 days was applied to the model SSH anomalies. The amplitude of the high-frequency part of the model surface variability is given in Fig. 15a, and its percentage contribution to the total variability is given in Fig. 15c. Figure 15b displays the corresponding Geosat high-frequency variability. Maximum values of eddy variability in the model are found close to the western boundary southeast of Cape Hat-

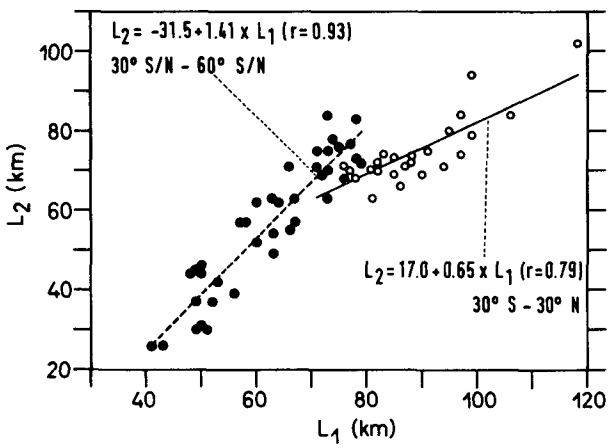

FIG. 12. Scatter diagram of L_2 against L_1 from all 10° areas given in Fig. 10. Numbers from areas poleward and equatorward of 30° latitude are indicated by solid and open circles. Note the clear break in the linear relation between both integral scales from midlatitudes and the subtropics at about 30° latitude.

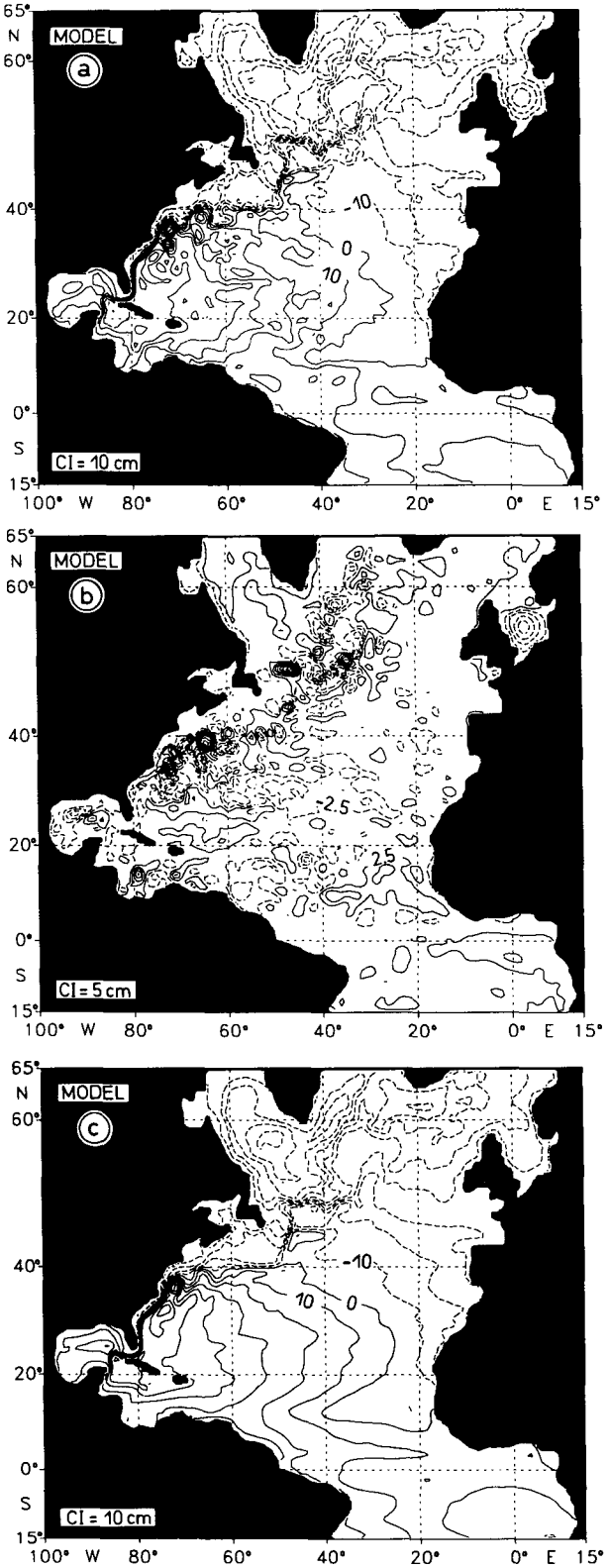

FIG. 13. (a) Model instantaneous sea-surface elevation ζ. Negative values are dashed and the first solid line indicates zero. Contour increment is 10 cm. (b) Same as (a), but for the surface elevation anomaly ζ'. Contour increment is 5 cm. (c) Model 3-year mean surface elevation $\bar{\zeta}$. Contour increment 10 cm.

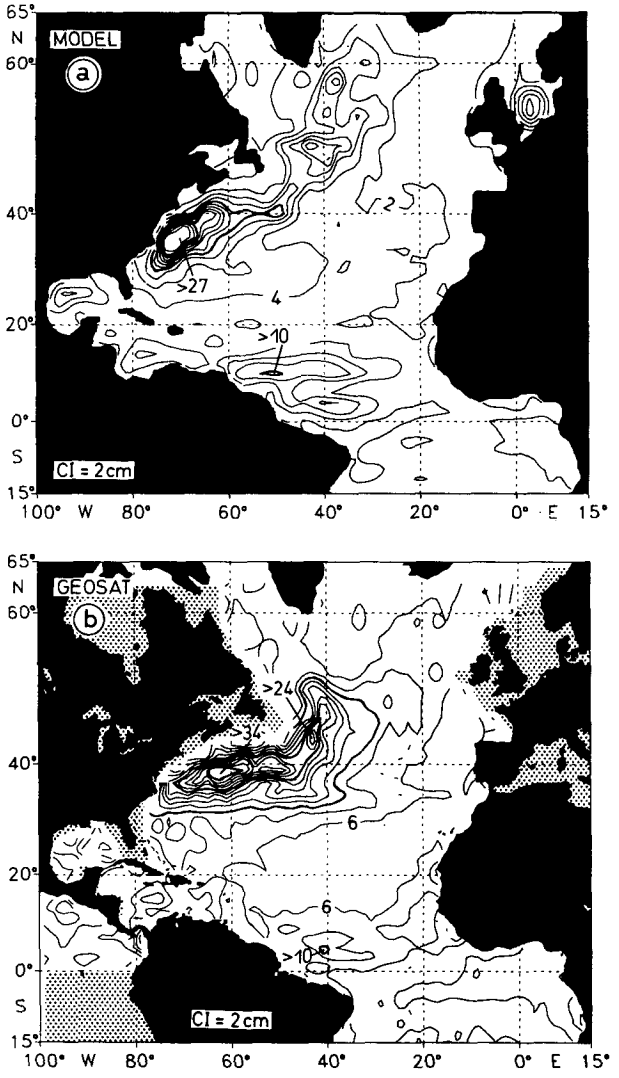

FIG. 14. (a) Model rms sea surface variability from three model years, estimated in 2° by 2° areas. Contour increment 2 cm. (b) Geosat rms sea surface variability as shown in Fig. 1a. Contour increment 2 cm.

teras corresponding to vigorous fluctuations of the current axis. Farther downstream the high-frequency variability is still enhanced. However, their percentage of the total is less than 10%. The latter finding holds for almost the entire model domain. In particular, the model eddy signal is less than observed by about a factor of 5. Despite those discrepancies all parts of the model ocean showing an increased percentage of high-frequency variability are also characterized by an increased percentage in the altimeter observations. In particular, this holds for the southern part of the subtropical gyre where an increased percentage of high-frequency variability occurs along a narrow belt in the westward-flowing portion of the subtropical gyre. This enhanced eddy activity extends from the Canary Islands across the basin into the Carribean where the percentage due to short-period fluctuations exceeds 70%. The model variability in the equatorial region is likewise characterized by a significant contribution from shorter time scales, and a high percentage is also found near 60°N, 30°W close to the Reykjanes Ridge. A comparison of model and Geosat results reveals that in most of the model regions with eddy variability being less than 10%, the percentage of high-frequency altimeter variability exceeds 50% (Fig. 26). As mentioned before, some fraction of that percentage has to be attributed to measurement noise (instrumental error plus residual errors from environmental corrections) that is absent in the model counterpart.

b. Comparison of wavenumber spectra and spatial eddy scales

For a comparison with the Geosat results meridional wavenumber spectra of the model surface elevation were estimated for 10° by 10° areas. Every fourth grid point zonally was used corresponding to a "cross-track" separation of 1.6° in zonal direction. The Geosat tracks are to first order aligned meridionally; close to the equator the deviation of the tracks from the NS direction is only 18°. Therefore, it is suitable to compare alongtrack spectra with model estimates in the meridional direction. Spectra were estimated with a sampling rate of 30 days and averaged over 3 years.

Model wavenumber spectra from three selected areas are shown in Fig. 16, representing (a) the tropical Atlantic (30°–40°W, 0°–10°N), (b) the Gulf Stream extension (60°–70°W, 30°–40°N), and (c) the northeastern Atlantic (20°–30°W, 40°–50°N), respectively. Included are the corresponding Geosat wavenumber spectra calculated along ascending and descending tracks. Generally, the comparison indicates a failure of the model to develop fluctuating eddy motions with amplitudes comparable to those from observations. Moreover, the model eddy field tends toward longer wavelengths in middle and high latitudes as compared to Geosat results. For wavelengths smaller than about 100 km the discrepancy is due to systematic errors in both datasets. While the Geosat spectra approach the altimeter noise level (which leads to "white" spectra at high wavenumbers), the biharmonic model friction, necessary to keep the model stable, acts selectively on small wavelength disturbances and leads to a rapid drop of energy at high wavenumbers. A comparison over the remaining wavenumber range, however, reveals similar characteristics of the spectra. In the equatorial region both model and Geosat spectra are red over the whole spectral domain. In higher latitudes both spectra show two distinct regimes, with a spectral relation close to k_1^{-5} beyond the cutoff wavenumber.

Model autocorrelation functions are drawn in Fig. 17 for the same areas as Fig. 16. Included are the corresponding alongtrack autocorrelation functions from Geosat (dashed curves). One important property of the oceanic variability is the systematic decrease of length scales toward high latitudes (see Fig. 11). An

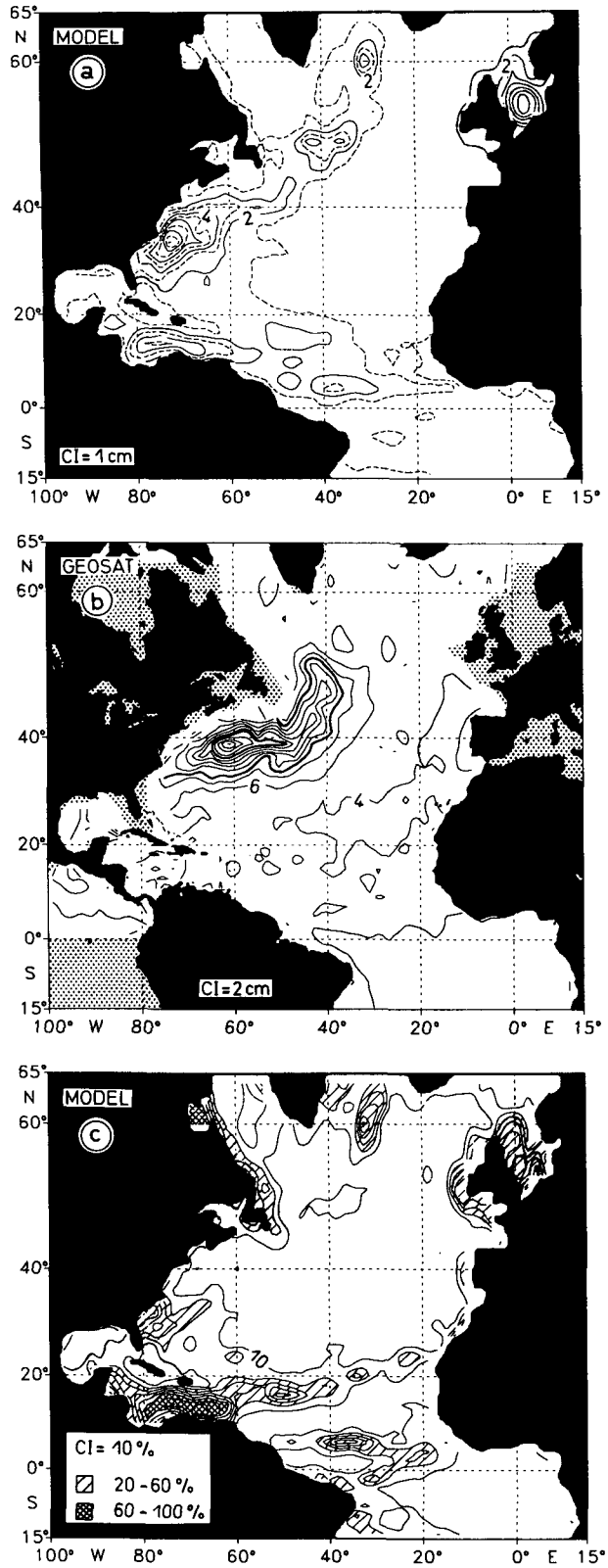

FIG. 15. (a) Same as in Fig. 14a, but model high-frequency variability with periods < 150 days. Contour increment 1 cm; solid lines correspond to contours in (b). (b) Geosat high-frequency variability with periods < 150 days, as given in Fig. 2a. Contour increment 2 cm. (c) Model percentage variability explained by high-frequency variability. Contour increment 10%; values exceeding 20% and 60% are hatched light and dark, respectively.

inspection of the model autocorrelation functions also indicates a decrease in the predominant model eddy scales with latitude. However, the decrease seems to be less pronounced than in the Geosat data. While there is some agreement between model and Geosat data in the equatorial region, the discrepancy seems to increase with latitude.

The latitudinal dependence of characteristic model length scales is exemplified in Fig. 18a, which shows zonal averages over 10° by 10° sites; included are the corresponding Geosat values for the Northern Hemisphere. The relative difference between model and Geosat scales is given in Fig. 18b. The lags of the first zero crossing show no significant difference equatorward of 30°N; in the poleward direction the difference increases, reaching about 50% at 60°N. In the linear (L_1) and quadratic (L_2) integral scales a similar increase of model–data discrepancy occurs toward high latitudes. However, a systematic difference also appears between both datasets in the tropics and subtropics. To a large degree this probably can be attributed to the poor signal-to-noise ratio of altimeter data and the corresponding bias of integral scales in these areas.

The basic conclusion drawn from this comparison is that the model is capable of resolving the energetic ocean structures in the tropical and subtropical Atlantic. The model resolution of $1/3° \times 2/5°$ appears to be too poor, however, to simulate the observed decrease of eddy scales with latitude. This results in a systematic failure of the model to simulate the energetic ocean eddies poleward of about 30°N. The influence of spatial grid resolution and horizontal friction on eddy dynamics was investigated in a sensitivity study with a similar primitive equation model but applied to an idealized model domain (Böning and Budich 1992). Decreasing the grid size by a factor of 2, from $1/3° \times 2/5°$ to $1/6° \times 1/5°$, along with the reduction of model friction, significantly enhanced the eddy activity in all parts of the model domain. Strongest differences in eddy kinetic energy (up to a factor of 5) and in eddy length scales, reduced by a factor of 2, occurred in the subpolar areas.

5. Are eddy characteristics universal?

The MODE and TOURBILLON observations gave some indication of a relation between eddy length scales and the first internal Rossby radius of deformation R_i (Mercier and Colin de Verdière 1985). Recently, Krauss et al. (1990) investigated the relation of characteristic eddy scales as derived from AVHRR infrared images. Based on local estimates of eddy scales from various sites north of 30°N, they reported a linear relation between the lag of the first zero crossing of au-

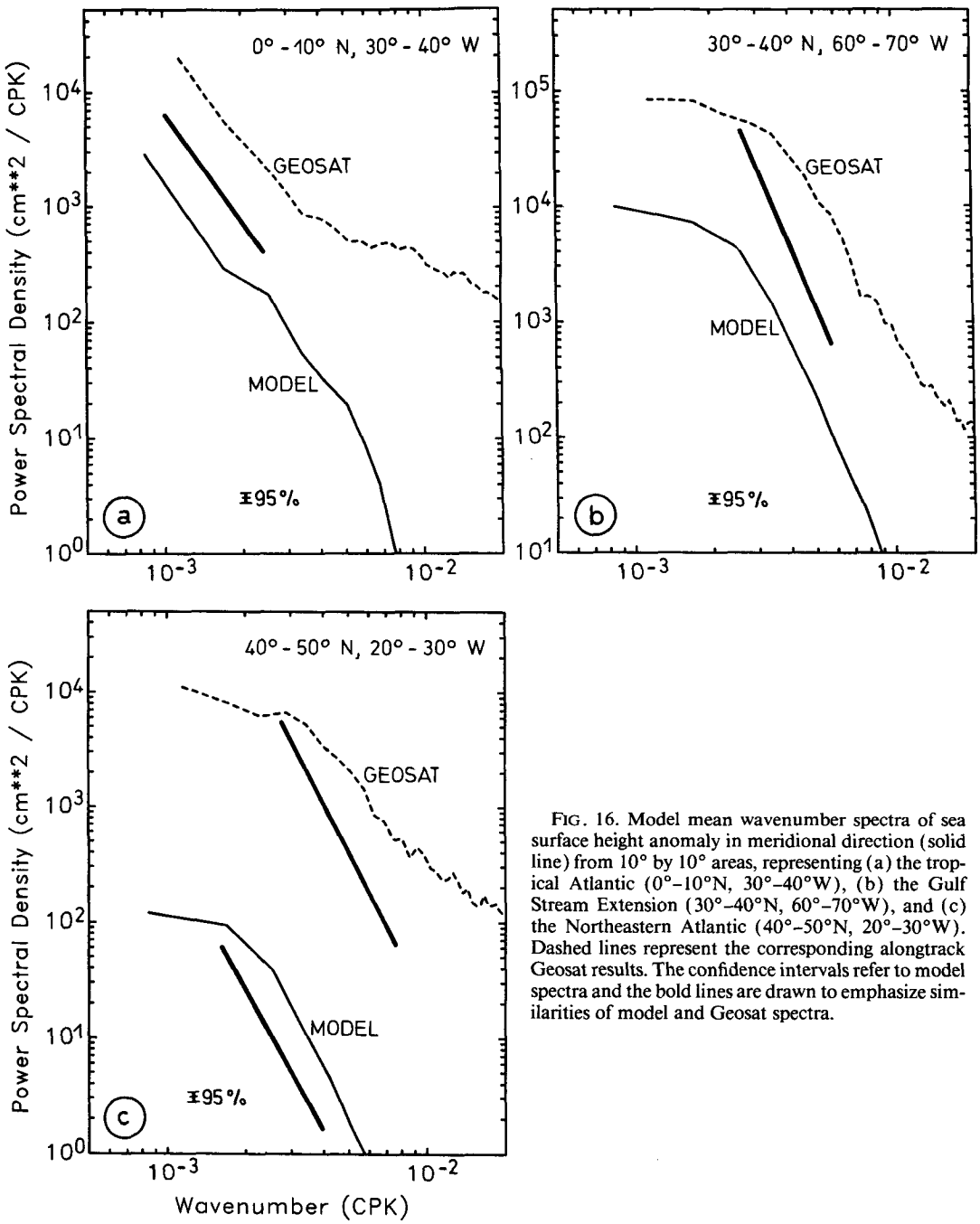

FIG. 16. Model mean wavenumber spectra of sea surface height anomaly in meridional direction (solid line) from 10° by 10° areas, representing (a) the tropical Atlantic (0°–10°N, 30°–40°W), (b) the Gulf Stream Extension (30°–40°N, 60°–70°W), and (c) the Northeastern Atlantic (40°–50°N, 20°–30°W). Dashed lines represent the corresponding alongtrack Geosat results. The confidence intervals refer to model spectra and the bold lines are drawn to emphasize similarities of model and Geosat spectra.

tocovariance functions and R_i: $L_0 = 31.5 + 0.96\pi R_i$. Deviations from a simple proportionality between integral scales and R_i were noted in the Geosat data analysis of Le Traon et al. (1990). It will be shown, however, that to a large degree this can be attributed to the degradation of integral scales in the low-energy areas of the subtropics.

A scatter diagram of L_1 (from Fig. 10) against the first deformation radius is shown in Fig. 19a. The values of R_i are adopted from the estimates of Emery et al. (1984) for the North Atlantic and Houry et al. (1987) for the South Atlantic and averaged over corresponding 10° by 10° boxes. Linear integral scales from areas poleward of 30° latitude (marked by open squares) show a linear relation with respect to R_i. Between 20° and 30° latitude there appears to be a somewhat different linear relation and close to the equator there apparently is no relation between L_1 and R_i. For values poleward of 30° latitude on both hemispheres a linear regression results in $L_1 = 40.6 + 1.15R_i$, with correlation $r = 0.85$. Doing the regression separately for the Southern and Northern hemispheres, gives slightly dif-

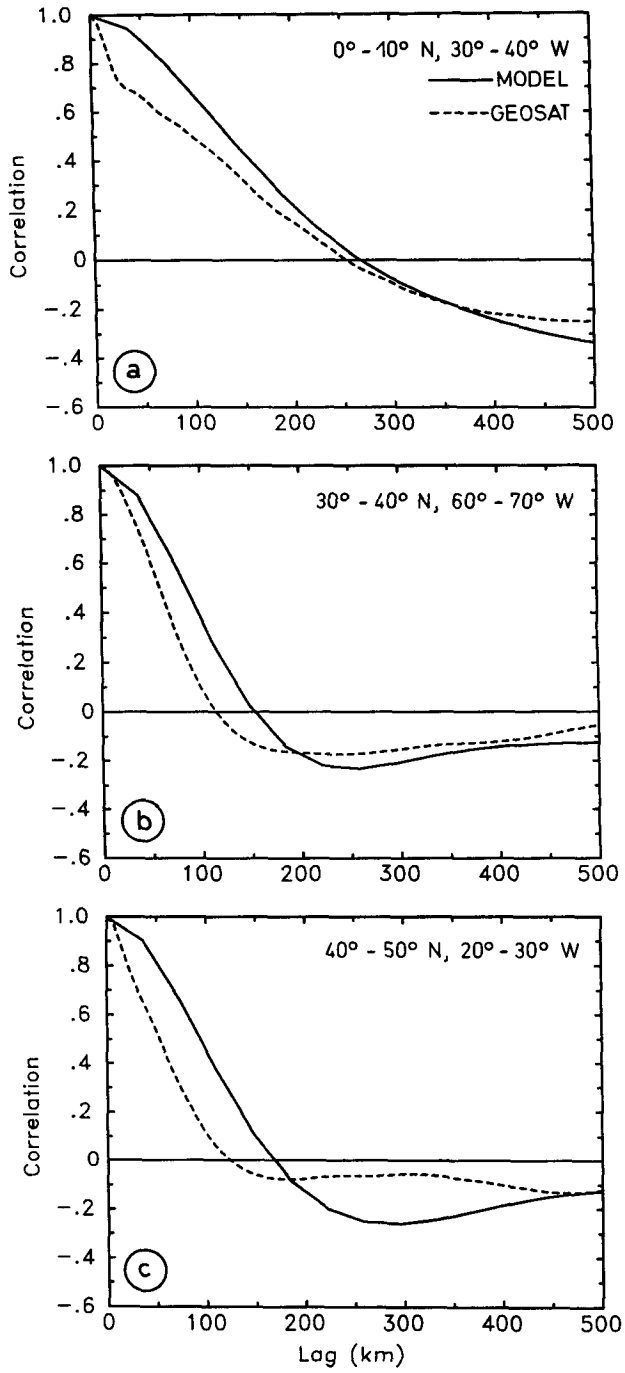

FIG. 17. Same as Fig. 16, but for the corresponding aurocorrelation functions.

ferent relations, with $L_1 = 41.5 + 0.93R_i$ ($r = 0.93$) for the North Atlantic and $L_1 = 38.3 + 1.38R_i$ ($r = 0.89$) for the South Atlantic.

As previously mentioned, the integral scales in the tropics and subtropics are likely to be degraded by measurement noise. In that area, however, no significant difference between Geosat and model data occurred in the lag of the first zero crossing. If we assume that in the tropics and subtropics the integral scales inferred from the model are representative for the oceanic signal, we may form a new integral scale L_1' by substituting the integral scales estimated from the noisy Geosat data by the model scales in that area. The result is shown in Fig. 19b; now a linear relation $L_1' = 34.0 + 1.4R_i$, ($r = 0.95$) characterizes the entire North Atlantic north of 10°N. A universal relation is also obtained when using the lag of the first zero crossing L_0 from Geosat (only values with pronounced zero crossing have been used). In Fig. 19c a linear regression leads to $L_0 = 79.2 + 2.2R_i$ ($r = 0.91$) for the entire Atlantic between 60°S and 60°N outside the equatorial region (10°S to 10°N).

The striking fact of a linear relation between the modified L_1' and R_i in the North Atlantic and between L_0 and R_i over the entire Atlantic Ocean obviously bears important dynamical implications. It should be noted that the bias of integral scales in the low-energy areas of the subtropics can severely mask the underlying relation with R_i. The use of integral scales can therefore be misleading in those areas. In addition, the peculiarities of the eddy scales in the subtropics reinforce our conclusion that the wavenumber spectra in those areas are severely distorted by measurement errors.

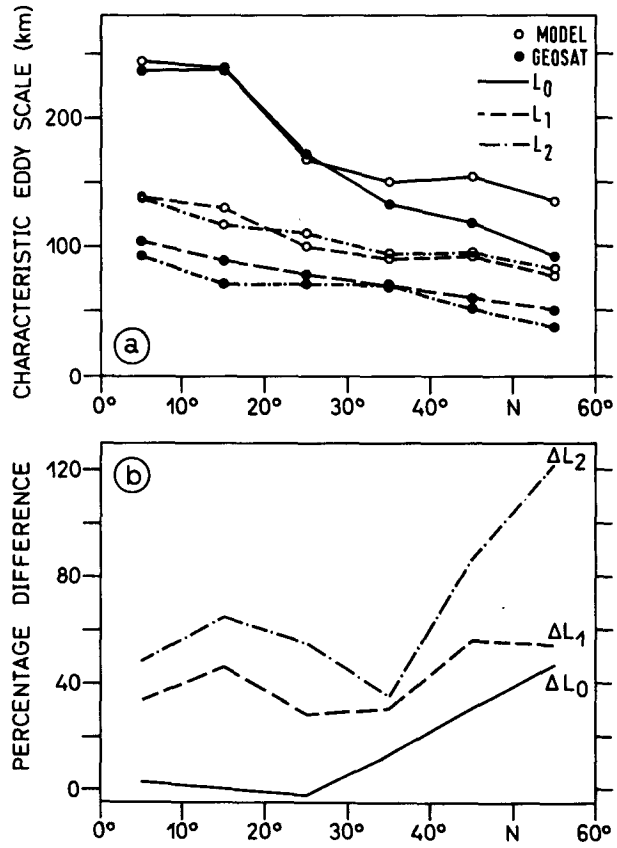

FIG. 18. (a) Zonal averages of characteristic eddy scales L_1, L_2, and L_0 inferred from model and Geosat data for the Northern Hemisphere and (b) their relative differences.

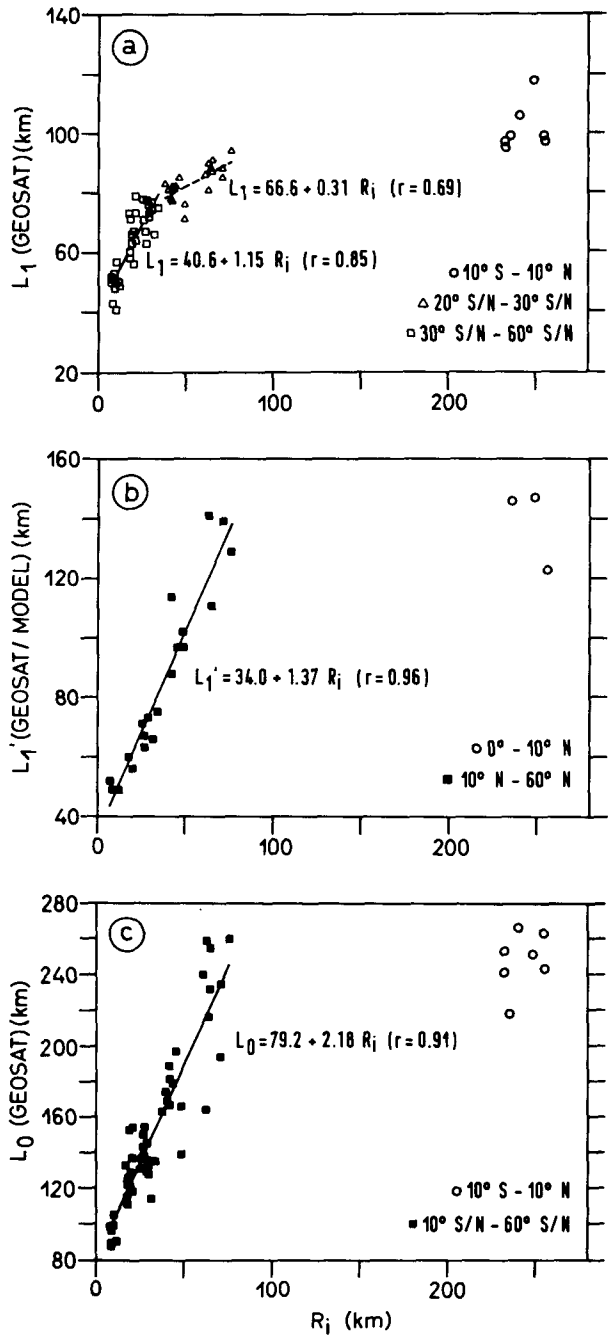

FIG. 19. (a) Scatter diagram of linear (L_1) integral scales from Geosat data over the entire Atlantic (see Fig. 10) against the corresponding Rossby radii of the first baroclinic mode derived from values given by Emery et al. (1984) for the North Atlantic, and by Houry et al. (1987) for the South Atlantic. Values poleward (squares) and equatorward (triangles) of 20°S and 30°N are significantly linearly related to the Rossby radius outside the equatorial region 10°S–10°N. In the equatorial region no relation is found. (b) Same as (a), but only for the North Atlantic with Geosat linear integral scales L_1 from areas equatorward of 30°N substituted by the corresponding values from model data. A linear relation between L_1' (Geosat plus model) and R_i is found poleward of 10°N. (c) Same as (a), but for the lag of the first zero crossing L_0 of the alongtrack Geosat autocorrelation function, revealing a close linear relation of L_0 with R_i over the entire Atlantic Ocean remote from the equator (10°S–10°N).

Therefore, the altimeter data give no evidence for deviations from a universal wavenumber spectrum of oceanic mesoscale variability.

A linear relation between eddy scales and R_i could be expected if baroclinic instability represents the predominant eddy generation mechanism. The existence of such a relation and the indication of a universal wavenumber spectrum over the entire Atlantic imply that dynamical processes that control the eddy size are similar everywhere. It also suggests that baroclinic instability may represent an important source of eddy energy not only close to boundary currents and frontal structures but also in the interior basin.

6. Summary and conclusions

We have used 58 repeats of Geosat ERM altimeter data to study characteristics of the ocean mesoscale variability, and, in particular, its geographical dependence. To reinforce our conclusions drawn from Geosat data and to document that altimeter data can indeed be used for a critical model test, results are compared to those from a high-resolution primitive equation model of the tropical and North Atlantic Ocean.

From Geosat sea surface height (SSH) anomalies the rms sea surface variability was estimated within 2° by 2° boxes from various spectral frequency bands. The analysis reveals that along major current systems a high percentage (>60%) of the total variability is due to variability on eddy time scales with periods < 150 days. The variability on annual time scale is only significant (>40%) in the equatorial region; there, it is associated with the seasonal reversal of the North Equatorial Counter Current.

Alongtrack wavenumber spectra were estimated over 10° by 10° areas and characteristic eddy length scales were derived from the corresponding autocovariance functions. Compared to Fu (1983a) and FZ a much larger area of the Atlantic Ocean is characterized by wavenumber spectra that can be represented by a relation of k_1^{-4} to k_1^{-5}. Only in those parts of the ocean where the rms variability in the eddy-containing frequency band is less than 5 cm, we find wavenumber spectra with slopes similar to the k_1^{-2} power law reported by Fu (1983a) and FZ for low-energy areas of the oceans. The larger extent of these anomalous areas in the earlier studies has to be regarded as an effect of the analysis scheme, in particular, that of the meridional extension of analyzed arc segments. Due to the inhomogeneity of eddy statistics with respect to latitude, estimates of wavenumber spectra over arc segments substantially longer than the variation length scale of the eddy field will ultimately lead to a flattened spectrum.

There are various indications that for the very low energy areas, such as between 20°S and 30°N, the departure from a −4 to −5 power law represents effects of measurement errors rather than an ocean signal. There the rms variability barely exceeds the altimeter

noise level; autocorrelation functions from those areas show degradations at small lags that are characteristics for measurement noise and give rise to an anomalous behavior of integral scales. We conclude that the altimeter data do not provide conclusive evidence of a significant departure from k_1^{-4} to k_1^{-5} type spectra. This lends support to the hypothesis that those spectral slopes, corresponding to the k_1^{-3} power law of geostrophic turbulence, may represent a universal characteristic of the ocean eddy field; it suggests that dynamical factors controlling eddy generation and interactions are similar over the basin and are independent of the eddy energy level.

From autocorrelation functions a pronounced decrease in characteristic eddy length scales is found from the equator toward high latitudes. The reduction of eddy scales toward boundary currents is comparatively weak. The zero crossing L_0 shows a linear relation with the internal Rossby radius R_i over the entire Atlantic Ocean outside the equatorial region (10°S to 10°N). This likewise holds for the integral scale L_1 poleward of 30° latitude in both hemispheres, and also for the entire North Atlantic north of 10°N if the integral length scales in the subtropics are substituted by the equivalent scales derived from the eddy-resolving model. The linear relation between eddy length scales and R_i confirms and extends earlier results from SST data in the North Atlantic (Krauss et al. 1990). It appears consistent with the similarity of the wavenumber spectra near ocean boundaries and in the interior basin and suggests that baroclinic instability is the leading mechanism in generating eddy variability, not only close to boundary currents and frontal regimes but also in the less energetic interior of the ocean.

The model–data comparison generally suggests that the model gives a first-order description of the regional distribution of eddy variability in the North Atlantic. In agreement with the observational evidence, high variability characterizes the Gulf Stream and the North Atlantic Current system, and enhanced variability occurs in the equatorial region. However, the amplitude of the variability in the model is systematically lower (up to a factor of 4) than has been found from Geosat observations. The model seems capable to simulate eddy characteristics in the lower latitudes. The model resolution of $1/3° \times 2/5°$, however, appears to be too poor to simulate the marked decrease in characteristic eddy length scales toward high latitudes, which lead to a systematic departure from space–time characteristics of model and Geosat data in the northern model domain. The model sensitivity study of Böning and Budich (1992) suggest that the increase of spatial grid resolution will serve to reduce much of the model–data discrepancies in middle and high latitudes. With the finer grid size of $1/6° \times 1/5°$ a substantially increase in model eddy activity takes place with much more realistic length scales.

Aside from the model verification, the data–model comparison bears some important implications with respect to future assimilation studies based on quasi-synoptic altimeter data, which are frequently discussed with respect to satellite data acquisition. It seems important that the dynamical model and the data coverage both sufficiently resolve the spatial characteristics of the mesoscale. The present comparison indicates that a significantly higher than $1/3°$ by $2/5°$ grid resolution has to be used poleward of 30°, in order to let the model "feel" the data. Another conclusion might be drawn with respect to satellite sampling requirements. According to White et al. (1990), it is the cross-track spatial data resolution rather than the alongtrack resolution that matters for assimilation experiments. Given that characteristic eddy length scales vary according to the internal Rossby radius, the cross-track resolution of altimeter satellite sampling schemes should be of the order of the Rossby radius in order to sufficiently constrain the model wavenumber characteristics in assimilation studies.

Acknowledgments. The authors are grateful to J. Willebrand for the stimulation of this study and many fruitful discussions. The help of R. Budich and R. Döscher in running the eddy-resolving model on the CRAY X-MP of Kiel University is appreciated. We also thank A. Schurbohm for assistance with the figures and S. Trier for help with the manuscript. This study was supported by the Bundesminister für Forschung und Technologie (Grant 07 KFT 460) and the "Deutsche Forschungsgemeinschaft" (SFB 133).

REFERENCES

Arhan, M., and A. Colin de Verdiere, 1985: Dynamics of eddy motions in the eastern North Atlantic. *J. Phys Oceanogr.*, **15,** 153–170.

Auer, S. J., 1987: Five-year climatological survey of the Gulf Stream System and its associated rings. *J. Geophys. Res.*, **92,** 11 709–11 726.

Böning, C. W., and M. D. Cox, 1988: Particle dispersion and mixing of conservative properties in an eddy-resolving model. *J. Phys. Oceanogr.*, **18,** 320–338.

——, and R. G. Budich, 1992: Eddy dynamics in a primitive equation model: Sensitivity to horizontal resolution and friction. *J. Phys. Oceanogr.*, **22,** 361–381.

——, R. Döscher, and R. G. Budich, 1991: Seasonal transport variation in the western subtropical North Atlantic. *J. Phys. Oceanogr.*, **21,** 1271–1289.

Bryan, K., 1969: A numerical method for the study of the circulation of the World Ocean. *J. Comput. Phys.*, **4,** 347–376.

Bryan, F. O., and W. R. Holland, 1989: A high-resolution simulation of the wind- and thermohaline driven circulation in the North Atlantic Ocean. P. Müller and D. Henderson, Eds. Parameterization of small-scale Processes, *Proc. 'Aha Huliko'a,* Hawaiian Winter Workshop, University of Hawaii at Manoa, 99–115.

Charney, J. G., 1971: Geostrophic turbulence. *J. Atmos. Sci.*, **28,** 1087–1095.

Cheney, R. E., J. G. Marsh, and B. D. Beckley, 1983: Global mesoscale variability from repeat tracks of SEASAT altimeter data. *J. Geophys. Res.*, **88,** 4343–4354.

——, B. C. Douglas, R. W. Miller, D. L. Porter, and N. S. Doyle, 1987: GEOSAT altimeter geophysical data record user handbook, NOAA Tech. Mem. NOS NGS-46, Natl. Ocean Surv., Rockville, Md., 32 pp.

Cox, M. D., 1984: A primitive equation, 3-dimensional model of the ocean. GFDL Ocean Group Tech. Rep. No. 1, GFDL/Princeton University, 143 pp.

Cox, M. D., 1985: An eddy resolving numerical model of the ventilated thermocline. *J. Phys. Oceanogr.*, **15**, 1312–1324.

Daniault, N., and Y. Menard, 1985: Eddy kinetic energy distribution in the Southern Ocean from altimetry and FGGE drifting buoys. *J. Geophys. Res.*, **90**, 11 877–11 889.

Dantzler, H. L., Jr., 1977: Potential energy maxima in the tropical and subtropical North Atlantic. *J. Phys. Oceanogr.*, **7**, 512–519.

DeMey, P., and A. Robinson, 1987: Assimilation of altimeter eddy fields in a limited area quasigeostrophic model. *J. Phys. Oceanogr.*, **17**, 2280–2293.

Didden, N., and F. Schott, 1992: Seasonal variations in the western tropical Atlantic: Surface circulation from GEOSAT altimetry and WOCE model results. *J. Geophys. Res.*, in press.

——, and D. Stammer, 1991: On the influence of tropospheric water vapor corrections on GEOSAT altimetry in the North Atlantic ocean. (to be submitted).

Douglas, B. C., D. C. McAdoo, and R. E. Cheney, 1983: Oceanographic and geophysical applications of satellite altimetry. *Rev. Geophys.*, **25**, 875–880.

Emery, W. J., 1983: On the geophysical variability of the upper level mean and eddy fields in the North Atlantic and North Pacific. *J. Phys. Oceanogr.*, **13**, 269–291.

——, W. G. Lee, and L. Magaard, 1984: Geographic and seasonal distribution of Brunt–Väisalä frequency and Rossby radii in the North Pacific and North Atlantic. *J. Phys. Oceanogr.*, **14**, 294–317.

——, G. H. Born, D. G. Baldwin, and Col. Norris, 1990: Satellite-derived water vapor corrections for GEOSAT altimetry. *J. Geophys. Res.*, **95**, 2953–2964.

Frankignoul, C., and P. Muller, 1979: Quasigeostrophic response of an infinite beta-plane ocean to stochastic forcing by the atmosphere. *J. Phys. Oceanogr.*, **9**, 104–127.

Fu, L.-L., 1983a: On the wavenumber spectrum of oceanic mesoscale variability observed by the SEASAT altimeter. *J. Geophys. Res.*, **88**, 4331–4341.

——, 1983b: Recent progress in the application of satellite altimetry to observing the mesoscale variability and general circulation of the oceans. *Rev. Geophys. Space Phys.*, **21**, 1657–1666.

——, and V. Zlotnicki, 1989: Observing ocean mesoscale eddies from GEOSAT altimetry: Preliminary results. *Geophys. Res. Lett.*, **16**, 457–460.

Gill, A. E., J. S. A. Green, and A. J. Simmons, 1974: Energy partition in the large-scale ocean circulation and the production of mid-ocean eddies. *Deep-Sea Res.*, **21**, 499–528.

Gordon, A. L., 1988: The South Atlantic: An overview of results from 1983–88 research. *Oceanogr.*, Nov., 12–17.

——, and T. N. Baker, 1980: Ocean transients as observed by GEOS 3 coincident orbits. *J. Geophys. Res.*, **85**, 502–506.

——, and W. F. Haxby, 1990: Agulhas eddies invade the South Atlantic: Evidence from Geosat altimeter and shipboard conductivity–temperature-depth survey. *J. Geophys. Res.*, **95**, 3117–3125.

Holland, W. R., 1978: The role of mesoscale eddies in the general circulation of the ocean–numerical experiments using a wind-driven quasigeostrophic model. *J. Phys. Oceanogr.*, **8**, 363–392.

Houry, S., E. Dombrowsky, P. DeMey, and J.-F. Minster, 1987: Brunt–Väisälä frequency and Rossby radii in the South Atlantic. *J. Phys. Oceanogr.*, **17**, 1619–1626.

Isemer, H.-J., and L. Hasse, 1987: *The BUNKER Climate Atlas of the North Atlantic Ocean. Vol. 2: Air–Sea Interactions.* Springer-Verlag, 256 pp.

Keffer, T., 1983: The baroclinic stability of the Atlantic North Equatorial Current. *J. Phys. Oceanogr.*, **13**, 624–631.

Koblinsky, C., 1988: Geosat vs. Seasat. *Eos Trans.* AGU, **69**, 1026.

Krauss, W., and C. W. Böning, 1987: Lagrangian properties of eddy fields in the northern North Atlantic as deduced from satellite-tracked buoys. *J. Mar. Res.*, **45**, 259–291.

——, R. Döscher, A. Lehmann, and Th. Viehoff, 1990: On eddy scales in the eastern and northern North Atlantic Ocean as function of latitude. *J. Geophys. Res.*, **95**(C10), 18 049–18 056.

Le Group Tourbillon, 1983: Studies of mesoscale eddies in the North East Atlantic. *Deep-Sea Res.*, **30**, 475–511.

Levitus, S., 1982: *Climatological Atlas of the World Ocean.* NOAA Tech. Paper **3**, 173 pp.

LeTraon, P. Y., M. C. Rouquet, and C. Boissier, 1990: Spatial scales of mesoscale variability in the North Atlantic as deduced from Geosat Data. *J. Geophys. Res.*, **95**(C11), 20 267–20 286.

McDowell, S. E., P. Rhines, and T. Keffer, 1982: North Atlantic potential vorticity and its relation to the general circulation. *J. Phys. Oceanogr.*, **12**, 1417–1436.

McWilliams, J. C., E. D. Brown, H. L. Bryden, C. C. Ebbesmeyer, B. A. Elliot, R. H. Heinmitter, B. L. Hua, K. D. Leaman, E. J. Lindstrom, J. R. Luyten, S. E. McDowell, W. B. Owens, H. Perkins, J. F. Price, L. Regier, S. C. Riser, H. T. Rossby, T. B. Sandford, C. Y. Shen, B. A. Taft, and J. C. Van Leer, 1983: The Local Dynamics of Eddies in the western North Atlantic. *Eddies in Marine Science*, A. R. Robinson, Ed. Springer Verlag, 92–113.

Menard, Y., 1983: Observations of eddy fields in the northwest Atlantic and northwest Pacific by SEASAT altimeter data. *J. Geophys. Res.*, **88**, 1853–1866.

Mercier, H., and A. Colin de Verdiere, 1985: Space and time scales of mesoscale motions in the eastern North Atlantic. *J. Phys. Oceanogr.*, **15**, 171–183.

MODE Group, 1978: The Mid-Ocean Dynamics Experiment. *Deep-Sea Res.*, **25**, 859–910.

Piola, A. R., H. A. Figueroa, and A. A. Bianchi, 1987: Some aspects of the surface circulation south of 20°S revealed by First GARP Global Experiment drifters. *J. Geophys. Res.*, **92**, 5101–5114.

Richarson, P. L., 1983: Eddy kinetic energy in the North Atlantic from surface drifters. *J. Geophys. Res.*, **88**, 4355–4367.

——, and T. K. McKee, 1984: Averaged seasonal variation of the Atlantic Equatorial Currents from historical ship drifts. *J. Phys. Oceanogr.*, **14**, 1226–1238.

Richman, J. G., C. Wunsch, and N. G. Hogg, 1977: Space and time scales of mesoscale motion in the western North Atlantic. *Rev. Geophys. Space Phys.*, **15**, 385–420.

Rhines, P. B., 1979: Geostrophic turbulence. *Ann. Rev. Fluid Mech.*, **11**, 401–441.

Sailor, R. V., and A. R. LeSchack, 1987: Preliminary determination of the GEOSAT radar altimeter noise spectrum. Johns Hopkins APL Tech. Dig., **8**(2), 182–183.

Schmitz, W. J., Jr., and W. R. Holland, 1986: Observed and modelled mesoscale variability near the Gulf Stream and Kuroshio Extension. *J. Geophys. Res.*, **91**, 9624–9638.

Schott, F. A., and C. W. Böning, 1991: The WOCE model in the western equatorial Atlantic: Upper-layer circulation. *J. Geophys. Res.*, **96**, 6993–7004.

Semtner, A. J., Jr., and R. M. Chervin, 1990: Environmental effects on acoustic measures of Global Ocean warming. *J. Geophys. Res.*, **95**, 12 973–12 982.

Spall, M. A., 1990: Circulation in the Canary Basin: A model-data analysis. *J. Geophys. Res.*, **95**, 9611–9628.

Treguier, A. M., 1992: Kinetic energy analysis of an eddy resolving, primitive equation model of the North Atlantic, *J. Geophys. Res.*, **97**, 687–701.

Wentz, F., 1990: User's manual allocated GEOSAT-SSM/I tape 1987–1989. RSS Tech. Rep. 100 190. Remote Sensing System, Santa Rosa, California, 4 pp.

White, W. B., C.-K. Tai, and W. R. Holland, 1990: Continuous assimilation of simulated Geosat altimeter sea level into an eddy-resolving numerical ocean model 1. Sea Level Differences. *J. Geophys. Res.*, **95**, 3219–3234.

Willebrand, J., R. H. Käse, D. Stammer, H.-H. Hinrichsen, and W. Krauss, 1990: Verification of GEOSAT sea surface topography in the Gulf Stream extension with surface drifting buoys and hydrographic measurements. *J. Geophys. Res.*, **95**, 3007–3014.

Wunsch, C. 1981: Low-frequency variability in the sea. *Evolution of Physical Oceanography: Scientific Surveys in Honor of Henry Stommel.* B. A. Warren and C. Wunsch, Eds., MIT Press, 342–374.

Wyrtki, K., L. Magaard, and J. Hager, 1976: Eddy energy in the oceans. *J. Geophys. Res.*, **81**, 2641–2646.

Zlotnicki, V., L.-L. Fu, and W. Patzert, 1989: Seasonal variability in global sea level observed with Geosat Altimetry. *J. Geophys. Res.*, **95**, 17 959–17 970.